INFRARED ABSORPTION STUDIES ON BARIUM TITANATE AND RELATED CRYSTALS

by

JAY TAYLOR LAST

B.S. University of Rochester
(1951)

SUBMITTED IN PARTIAL FULFILLMENT OF THE

REQUIREMENTS FOR THE DEGREE OF

DOCTOR OF PHILOSOPHY

at the

MASSACHUSETTS INSTITUTE OF TECHNOLOGY

Signature of Author .....
Department of Physics, March 27, 1956

Certified by .....
Thesis Supervisor

Accepted by .....
Chairman, Departmental Committee
on Graduate Students

INFRARED ABSORPTION STUDIES ON BARIUM TITANATE AND RELATED CRYSTALS

by

JAY TAYLOR LAST

Submitted to the Department of Physics on March 27, 1956 in partial fulfillment of the requirements for the degree of Doctor of Philosophy

ABSTRACT

The infrared absorption spectrum of $BaTiO_3$ has been measured for thin single crystals and for powder samples dispersed in pressed KBr disks. Absorption bands occur at 495 cm^{-1} and at about 340 cm^{-1} for single-crystal samples and at slightly higher frequencies for the pressed disks. These bands arise from normal vibrations of the TiO_3 group. A third vibration, a motion of Ba against the TiO_3 group, occurs below the available experimental range. A frequency of about 225 cm^{-1} is expected for this band on the basis of a comparison of the specific heat contributions of the observed bands with the measured low-temperature specific heat.

The effect of changes of crystal symmetry and structure on the infrared spectrum was investigated by making measurements on the 495 cm^{-1} band over a wide temperature range. As the crystal changes from the cubic to the tetragonal, orthorhombic, and rhombohedral structures, band splitting is observed which can be related to the change of crystal symmetry. A slight frequency splitting for vibrations along and at right angles to the polar axis in tetragonal $BaTiO_3$ has been observed using polarized radiation on a single-domain crystal. This splitting is due to the displacement of the Ti ion from a central position in the unit cell when the material becomes ferroelectric.

The spectra of the perovskite titanates, $SrTiO_3$, $PbTiO_3$, and $CaTiO_3$, and the perovskite niobates, $KNbO_3$ and $NaNbO_3$, have been found to be similar in general features to that of $BaTiO_3$. The slight differences in band frequency and structure observed are related to differences in unit cell size and symmetry. The spectra of the ilmenite titanates, $MgTiO_3$, $ZnTiO_3$, and $CdTiO_3$, differ in significant detail from those of the perovskite titanates due to the radically different structure of these materials.

Integrated band intensities have been measured and found to be in reasonable agreement with measurements on other oxide systems having vibrations in this spectral region. No anomalous changes in intensity have been observed at the cubic-tetragonal transition where $BaTiO_3$ becomes ferroelectric or at the lower temperature phase transitions.

Thesis Supervisor: Arthur R. von Hippel

Title: Professor of Electrophysics

Acknowledgment

The author is greatly indebted to Professor A. R. von Hippel for suggesting this problem, and for much helpful advice and encouragement.

It is a great pleasure to acknowledge the assistance and advice of Dr. Robert D. Waldron, group leader of the spectroscopy section of the Laboratory for Insulation Research, in all phases of this investigation. The cooperation of Dr. Peter W. Forsbergh, Jr., and Mr. W. B. Westphal is also gratefully acknowledged.

The $BaTiO_3$ crystals used were kindly supplied by Mr. V. Sils, Mr. H. Bradt, and Mr. J. Smiltens of the Laboratory for Insulation Research, crystals of $PbTiO_3$, $NaNbO_3$, and $KNbO_3$ by Dr. K. McKay, Mr. J.P. Remeika, Mr. E.M. Kelley, and Dr. M.A. Gilleo, of the Bell Telephone Laboratories, and a crystal of $SrTiO_3$ by the National Lead Company.

Mr. S.M. Kingsbury has rendered much appreciated aid in the procurement of apparatus, materials, and special facilities.

The author would like to thank the E.E. Machine Shop, under the direction of Mr. P. Kelleher, for their kind cooperation, and Mr. J. Mara, for drawing the figures in this thesis.

The author wishes to express his gratitude to the International Business Machines Corporation for support in the form of a fellowship, and to Dr. D.R. Young of I.B.M. for helpful discussions.

This investigation was made possible through support extended to the Laboratory for Insulation Research by the Office of Naval Research, the Army Signal Corps, and the Air Force.

TABLE OF CONTENTS

Table of Contents (cont.)

List of Figures

List of Figures (cont.)

List of Figures (cont.)

CHAPTER I

INTRODUCTION

The study of the spontaneous orientation of dipole moments in ferroelectrics and ferromagnetics is one of the long-range research projects of the Laboratory for Insulation Research.[1,2] In investigating the phenomena taking place in such complex materials as the titanates or ferrites, tools of nondestructive analysis are needed which can give information on atomic arrangements and interatomic forces in the crystal lattice. One of these tools is infrared spectroscopy. A first infrared study on ferrites has been carried through recently in this laboratory[3] and has given promise of locating cations in their oxygen surroundings. The present investigation is a complementary study on ferroelectrics which tries to establish how the infrared vibrational frequencies, and thus the interatomic forces, are affected by the onset of the ferroelectric state and by the various low-temperature phase transitions.

In contrast to the large amount of work which has been done by infrared spectroscopists on the absorption spectra of gases, few investigations have been carried out on solids, due in large part to problems of sample preparation, and to the difficulty in many cases of interpretation of the observed spectra. In the present investigation, in addition to specific information which can be gained on $BaTiO_3$, further progress can be made on the experimental problems of far infrared absorption measurements on solids, as well as obtaining information necessary for an increase in the understanding of the excitation of optically active lattice vibrations.

The experimental measurements carried out in this investigation can be divided into three groups: the absorption spectra of thin single crystals, the absorption spectra of powdered samples dispersed in pressed potassium bromide disks, and the reflection spectra of single crystals. The main emphasis has been placed on the measurement of the spectrum of $BaTiO_3$ because of intrinsic interest in this material and because of availability of structural data, low temperature specific heat measurements, and data on the electrical properties helpful for a detailed discussion of the infrared spectrum. Measurements have been carried out on several related materials where this would yield information valuable for an interpretation of the titanate spectrum.

1. Previous Infrared Measurements

The earliest infrared investigation of the high dielectric constant titanium-oxygen compounds was the measurement of the reflection spectrum of rutile TiO_2 by Liebisch and Rubens[4], in the wavelength region from the visible to 300 microns (μ) (Fig. 1). The observed spectrum consisted of broad bands centered at about 20 μ and 40 μ, and a region of high reflectivity at longer wavelengths. The high dielectric constant of this material has been related to these vibration bands.[5]

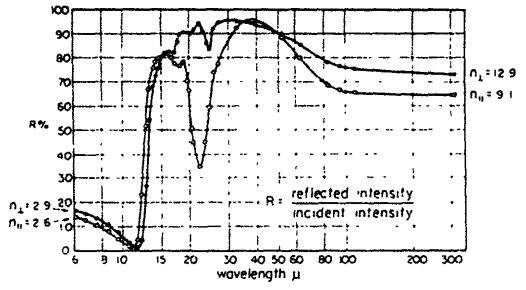

Fig. 1. Infrared reflection spectrum of rutile (after Liebisch and Rubens[4]).

Measurements by Mara et

al.[6] of the infrared absorption spectrum of powder samples of $BaTiO_3$ deposited on a KBr plate show bands in the same spectral region as the rutile bands (Fig. 2). The observed spectrum consisted of two strong bands, the higher frequency band centered near 550 cm^{-1} (18 μ), the lower starting near 450 cm^{-1} and reaching a maximum beyond 300 cm^{-1}. Near infrared absorption was observed, and was shown to be due to impurities. No change was observed in the spectrum of ceramic samples above the Curie point. The spectra of $BaTiO_3$, $SrTiO_3$, and hexagonal $BaTiO_3$ were found to be identical in the near infrared region from the visible to 600 cm^{-1}.

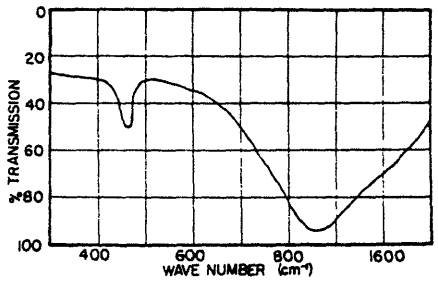

Fig. 2. Infrared absorption spectrum of powder $BaTiO_3$ (after Mara[6]).

Previous single crystal absorption measurements have been confined to the near infrared. Measurements by Hilsum[7] on single crystal $BaTiO_3$ indicated a weak band at 8.3 microns, and a strong absorption band beginning near 7 μ and continuing to a point of zero transmission at about 12 μ (Fig. 3). Similar measurements have been made by Levy et al.[8] on $SrTiO_3$, who observed an absorption shoulder at 5.5 μ, a narrow band at 7.5 μ, and an absorption edge beginning at about 5 μ and reaching zero transmission at about 11 μ.

2. Structure and Phase Transitions of $BaTiO_3$

Barium titanate, in the modification having unusual electrical

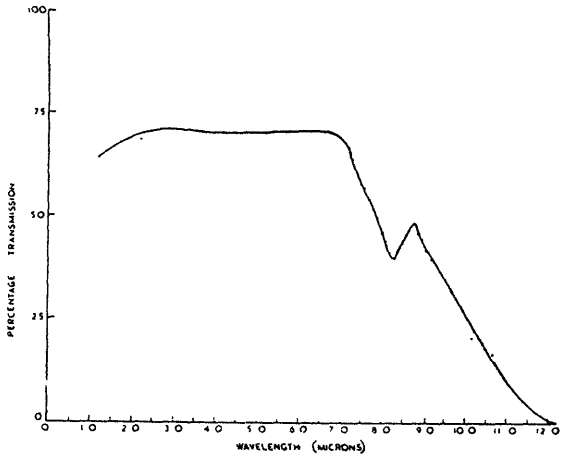

Fig. 3. Near infrared absorption spectrum of single crystal $BaTiO_3$, 0.094 mm in thickness (after Hilsum[7]).

properties, has a perovskite structure (Fig. 4). Above the Curie temperature of about 120°C, the lattice has cubic symmetry, with a Ti ion at the center of the unit cell, O ions centered on the six cube faces, and Ba ions on the cube corners. The structure can be described as a system of TiO_6 octahedra joined at the corners with the Ba ions placed in the interstitial positions between the octahedra.

As the cubic crystal is cooled through the Curie point, a polar axis develops along a [100] direction, and the elongation in this direction leads to a structure with tetragonal symmetry. At room temperature, the spontaneous polarization has a value of about 25×10^{-6} coulombs/cm^2 [9]; the dielectric constant is about 200 along the polar axis and about 5000 at right angles to this axis.[10] In general, a ferroelectric domain structure results because the polar axis can develop in several equivalent directions.

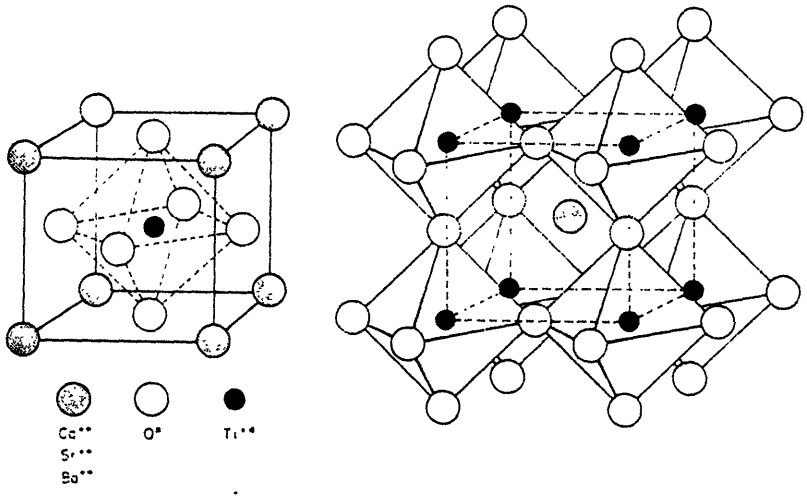

Fig. 4. The ideal perovskite structure.

(a) Unit cells centered around Ti^{+4} ions

(b) TiO_6 octahedra surrounding Ba^{+2} ion.

Near 0°C, the polar axis shifts to the [100] direction and at about -70°C to the [111] direction with a structural change to orthorhombic and then to rhombohedral. The material remains ferroelectric throughout.

The unit cell dimensions in the four phases, as investigated by Megaw[11], Vousden[12], and Rhodes[13] are listed in Table I. (In the orthorhombic phase, the unit cell is shown as monoclinic, with the orthorhombic "a" and "c" axes forming the face diagonals of the monoclinic cell.)

3. Determination of the Atomic Positions in $BaTiO_3$

X-ray diffraction measurements of the slight shifts of the atoms from symmetrical positions in the tetragonal unit cell have been made by

TABLE I

$BaTiO_3$ unit cell dimensions

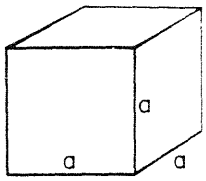 CUBIC (O_h) T > 120°C	a = 4.009 A
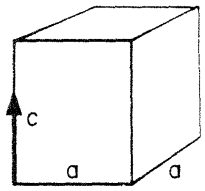 TETRAGONAL (C_{4v}) 5° < T < 120°C	a = 3.994 A c = 4.034 A c/a = 1.01 Polar axis : [100]
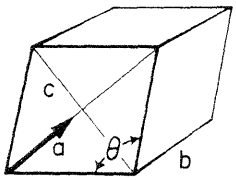 ORTHORHOMBIC (C_{2v}) -70° < T < 5°C	a = 5.682 A c = 5.669 A b = 3.990 A θ = 90° 8' Polar axis : [110]
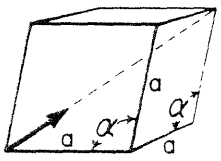 RHOMBOHEDRAL (C_{3v}) T < -70°C	a = 4.001 A α = 90° 14' Polar axis : [111]

Känzig[14] and by Evans.[15] Unfortunately, the X-ray intensity measurements do not lead to an unambiguous result, due to difficulties of separating co-ordinate and thermal oscillation parameters, and because of the strong scattering of the Ba ions. This difficulty led Evans to propose two models, the first with reasonable assumptions concerning the thermal oscillations which led to fair agreement between observed and calculated intensities, and the second with better intensity agreement but unreasonable temperature parameters.

Neutron diffraction measurements, where the scattering factors are more nearly equal and constant with angle, may overcome this ambiguity. Preliminary neutron diffraction measurements have been reported recently by Frazer et al.[16]

In Table II, the room temperature measurements of the atomic positions based on the model of Känzig, the two models of Evans, and the model given by Frazer based on neutron diffraction measurements are shown. In this tabulation, the Ba atom site is given as the reference point, and the displacements of the Ti ion, the O_I ion (the oxygen ion lying along the polar axis), and the O_{II} ion (at right angles to the polar axis) are listed. All of these models indicate a shift of the Ti atom to a point not midway between its two O_I neighbors. The Ti-O_I distances given by these various models are also tabulated.

The atomic shifts in $PbTiO_3$, a ferroelectric material which has a room-temperature structure similar to tetragonal $BaTiO_3$, have been determined recently by Shirane[17], using a combination of X-ray and neutron diffraction techniques. The results of this investigation are included in Table II.

Table II. Atomic Shifts in Tetragonal $BaTiO_3$ and $PbTiO_3$
(Relative to Ba and Pb)

	δTi	δO_I	δO_{II}	$Ti-O_I$ distances	
$BaTiO_3$ (Frazer)	- 0.056A	0.093A	0.056A	1.868A	2.166A
$BaTiO_3$ (Evans #1)	- 0.048	0.105	0	1.864	2.170
$BaTiO_3$ (Evans #2)	- 0.060	0.097	0.081	1.860	2.174
$BaTiO_3$ (Känzig)	- 0.056	0.129	0	1.832	2.202
$PbTiO_3$ (Shirane)	0.17	0.46	0.46	1.79	2.37

$BaTiO_3$: c = 4.034A; c/a = 1.01

$PbTiO_3$: c = 4.15A; c/a = 1.06

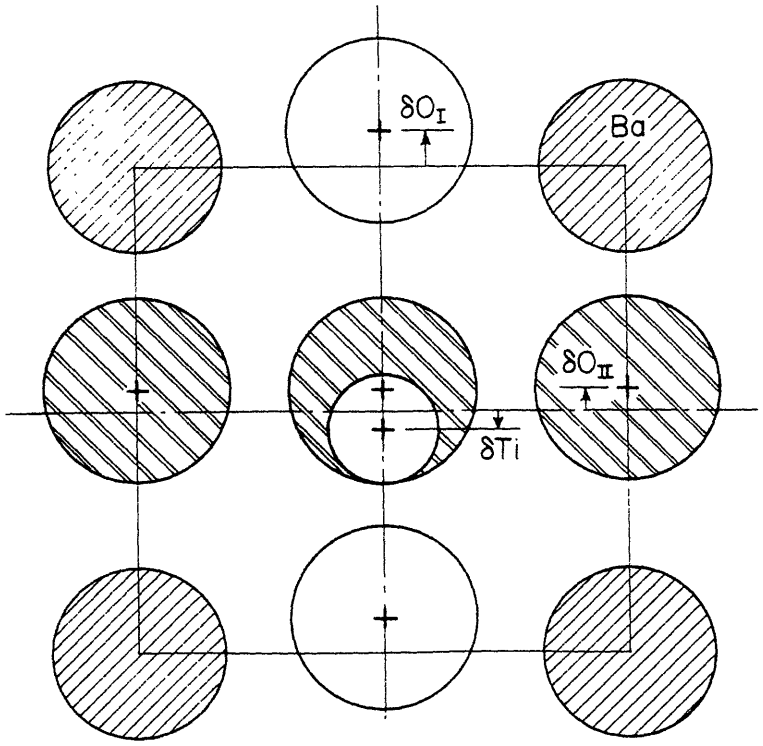

CHAPTER II

INSTRUMENTATION AND EXPERIMENTAL TECHNIQUES

1. Instrumentation

The spectra measured in this investigation were recorded with a Beckman IR-3 spectrophotometer, equipped with CaF_2, KBr, and KRS-5 prisms, providing a range of operation extending from the visible to about 300 cm^{-1} (33 microns).

This spectrophotometer is a single beam instrument, with a Nernst glower light source, a double monochromator dispersing system, and a thermocouple signal detector. The instrument was calibrated by recording the spectra of gases which have been measured with considerable accuracy on grating instruments.[18] The calibration drift is negligible. The whole instrument can be evacuated to remove interference caused by atmospheric absorption by water vapor and carbon dioxide, and is held at controlled temperature by circulating water from a constant temperature bath.

The light beam is chopped near the source at a frequency of 10 cycles/sec., and the signal detected by the thermocouple is fed to a tuned 10 cycle amplifier through a precision transformer which provides an impedance match between receiver and amplifier. The amplified 10 cycle signal is rectified and further amplified by a D.C. amplifier. A thermocouple signal of 2.5×10^{-9} volts can be recorded. The spectra are presented on a Brown recorder, coupled to the prism wavelength drive by a nonlinear optical-electrical system to permit the presentation of data linear either in frequency or wavelength.

The instrument was used in its normal double monochromator operation with the CaF_2 and KBr prisms, from the visible to about 425 cm^{-1}. At the slit widths normally employed, the spectral resolution ranged from about 5 cm^{-1} at 1000 cm^{-1} to about 10 cm^{-1} at 500 cm^{-1} with the KBr prisms.

Due to the low light source intensity and the fall-off of thermocouple sensitivity at long wavelengths, the instrument was used as a single monochromator with a KRS-5 prism in the frequency range from 500 to 300 cm^{-1}. A coarse ground CaF_2 residual ray plate was used to remove short wavelength radiation from the beam. The stray light was less than 5% over the whole range. The spectral resolution was about 20 cm^{-1} in the KRS-5 region. In this region, we increased the signal amplification about fourfold by slightly modifying the final stage of the D.C. amplifier. In order to keep the signal to noise ratio low, the amplifier time constant was increased, and with it the scanning time in this region.

The IR-3 is designed primarily as an instrument for the study of the spectra of gases and liquids. In order to provide for the installation of the auxiliary equipment required for the study of solids, a longer sample compartment was installed.

2. Auxiliary Equipment

A Dewar microcell, designed by R. D. Waldron, was used in the investigation of the spectra of small single crystals between -190°C and about +175°C (Fig. 5). Hot oil, dry ice and methyl alcohol, and liquid nitrogen were used to provide this temperature range. The slit image was reduced at a ratio of about 15 to 1 by the use of parabolic KBr and KRS-5

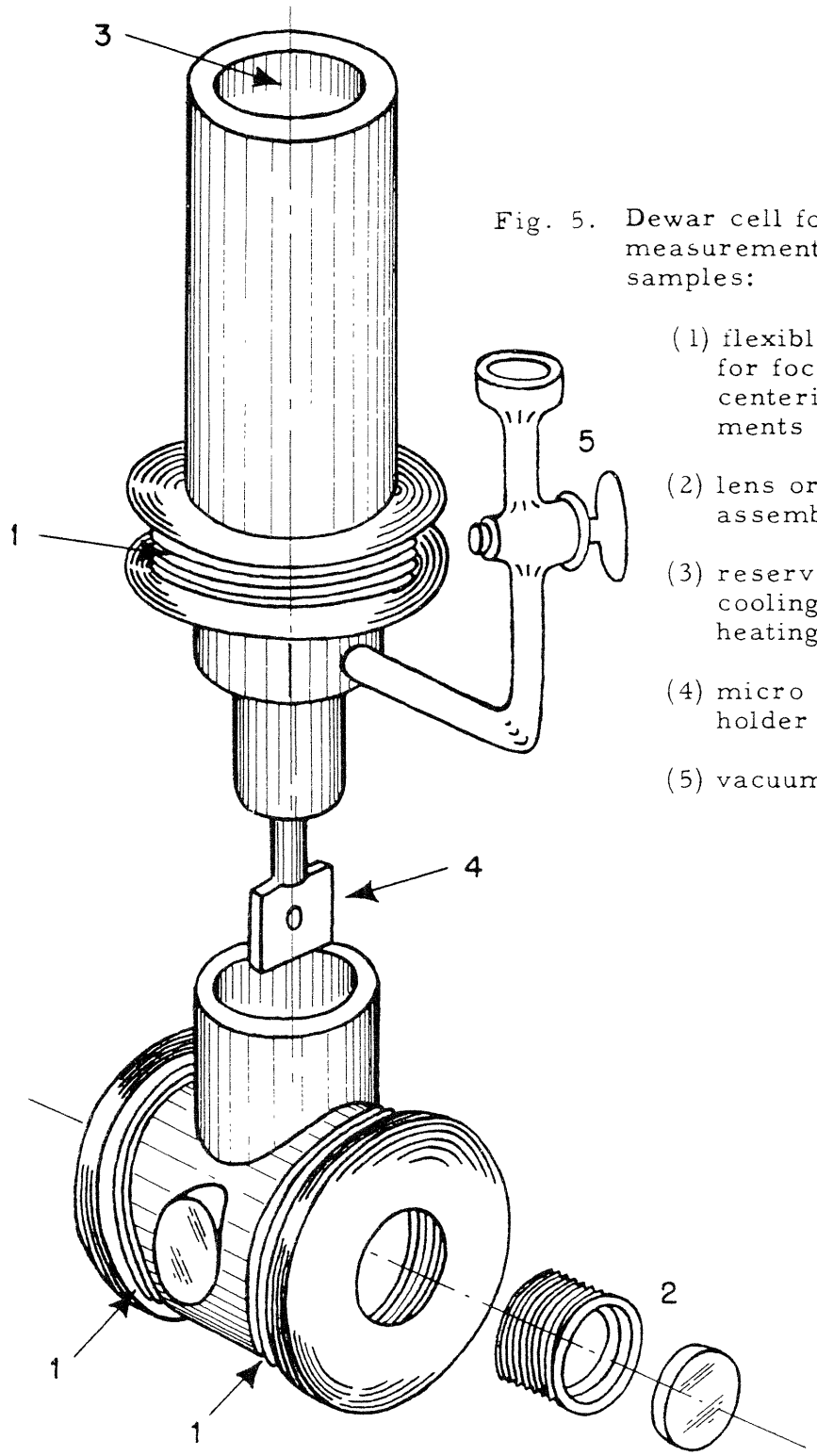

Fig. 5. Dewar cell for infrared measurements of solid samples:

(1) flexible bellows for focusing and centering adjustments

(2) lens or window assembly

(3) reservoir for cooling- or heating-bath

(4) micro sample holder

(5) vacuum line

lenses. With the KBr lenses, about 55% of the incident beam could be passed through an aperture 1.5 mm high placed at the focal point of the microcell; with KRS-5 lenses, about 30% of the beam could be passed.

For the investigation of the low-temperature spectra of larger samples, a Dewar cell with AgCl windows was used, similar to that described by Wagner and Hornig.[19]

For single crystal reflection measurements, the reflection system illustrated in Fig. 6 was used. It permitted measurement of reflectivity at angles ranging from about normal incidence to about 80°, without deflecting the beam.

An infrared polarizer was constructed from four sheets of AgCl set at the Brewster angle; its efficiency was about 90% to about 20 microns.

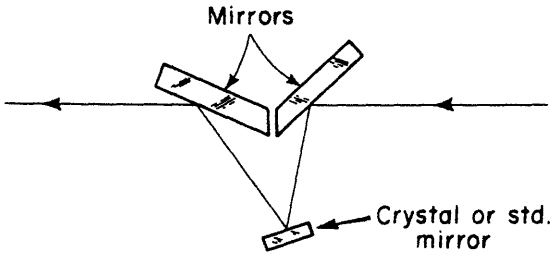

Fig. 6. Mirror arrangement for crystal reflection measurements.

3. Preparation of Thin Single-Crystal Samples

The most difficult experimental problem in the study of vibration spectra of single crystals is the preparation of samples thin enough to

transmit a measurable quantity of light in the absorption band. In general, for ionic crystals the thickness must be of the order of one micron. Methods were developed for preparing and handling $BaTiO_3$ crystals of this thickness.

A crystal grinder and polisher was constructed which could be used for the preparation of crystals as thin as 15 microns. The crystal was cemented with optical pitch to a thick piece of plate glass, and placed in an inverted position on the polisher support (Fig. 7). The polishing lap was cemented to a second piece of plate glass fastened to a rotatable cylinder which could be raised in very small increments with a micrometer screw. This permitted an accurate control of the pressure exerted on the crystal by the lap during polishing, and helped greatly to reduce crystal breakage.

Since crystals thus prepared were still an order of magnitude too thick for the measurement of the lattice vibration absorption, etching

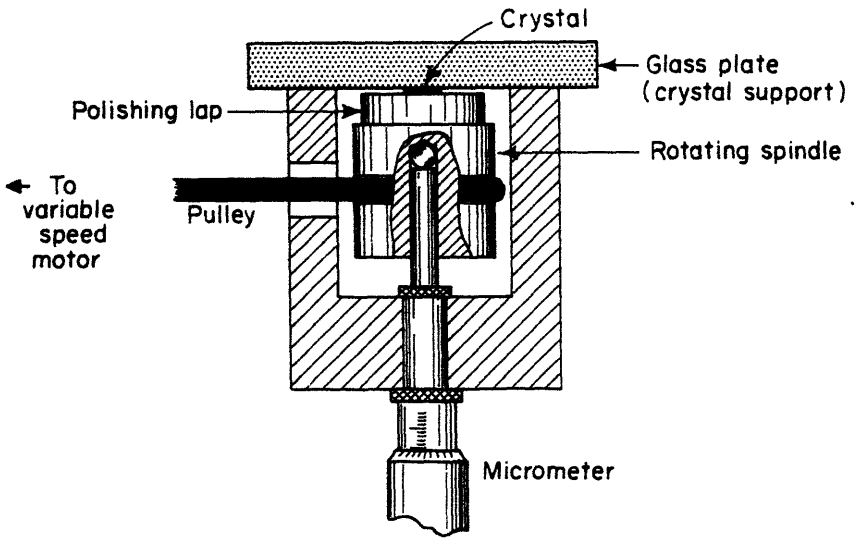

Fig. 7. Thin crystal polisher.

techniques using phosphoric acid were develcped. The samples were etched in acid heated above the Curie temperature to prevent the selective etching of domains. In the cubic phase, the etching proceeded very smoothly, with an etching rate of about one micron a minute at a temperature of 130°C.

A low-power microscope was used to measure the crystal thickness before etching. The crystals, grown by V. Sils and H. Bradt of this laboratory, had an initial thickness of 25 to 100 microns.

In initial etching attempts, the crystals were placed in a platinum screen basket suspended in the etching bath. After etching, the crystals were transferred from the basket to a sample holder by floating them on water. The surface tension of the water was reduced by adding methyl alcohol. Crystals as thin as 2 microns were prepared by this technique.

Later, the crystal was supported in the acid bath by a recently developed silicone-teflon tape*, which could withstand several hours immersion in hot phosphoric acid without deterioration. The crystal was held between two pieces of tape with their adhesive sides joined (Fig. 8). Windows were cut over the area to be etched. Pieces of platinum wire were bent around the tape to prevent it from warping during immersion in the acid bath. This method of sample support greatly facilitates the handling of very thin crystals, since they can be left in the tape support and mounted directly in a sample holder suitable for absorption measurements. Crystals 1.5 microns thick were prepared by this method.

Soaking the crystal for a few minutes in cold acid before placing them in the hot acid bath helped to eliminate air spaces between the pieces of tape at the crystal edges. If air bubbles were present, they

---

* Minnesota Mining and Manufacturing Company, St. Paul, Minnesota.

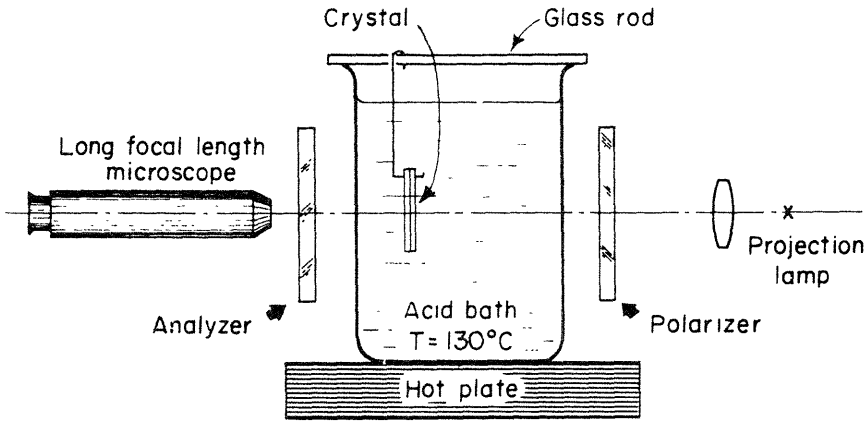

(a)

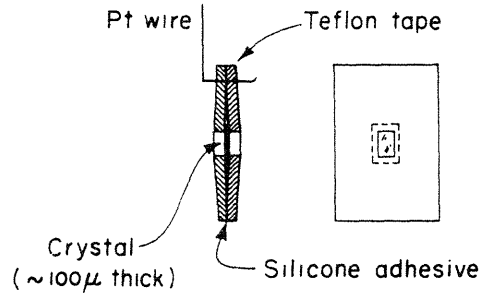

(b)

Fig. 8. (a) Thin crystal etching apparatus. (b) Sampleholder.

expanded in the hot acid and collected on the crystal surface. The crystal then fractured or became etched non-uniformly in many cases. This could be prevented by lifting the crystal out of the bath for a few seconds to remove the bubbles. After the crystals were etched to the proper thickness, they were rinsed in water, dried, and any acid remaining on the tape or crystal was neutralized by exposing the crystal holder to ammonia fumes for a few seconds.

The method used for determining the crystal thickness during etching is shown in Figure 8. The crystal etching bath was placed between crossed polarizers, and the crystal observed with a low power microscope. In order to measure thickness, the bath temperature was lowered for a few seconds below the Curie point, and the crystal thickness estimated from the birefringence colors which appear when the crystal is tetragonal.

Under crossed polarizers, a $BaTiO_3$ crystal with its polar axis in the crystal plane will exhibit blue and red birefringence colors until it is below 10 microns thick. Between about 8 microns and 3 microns the birefringence color changes from a dark to a light yellow. At 2 microns, the crystal is grey-white, and at 1.5 microns dark grey. Under parallel polarizers, a crystal 2 microns thick appears slightly yellow, and becomes grey-white at about 1.5 microns.

The crystals obtained by this etching technique were sufficiently plane-parallel to permit the observation of interference bands in the near infrared. An accurate value of the crystal thickness could be obtained from the frequency separation of these bands and the known value of the index of refraction.

About 25 crystals were etched by the above techniques. Photomicrographs of representative crystals are shown in Figs. 9 and 10. The crystal area is about 2x1 millimeter, and the thickness about 1.5 microns. Figure 9 shows a typical mixed domain crystal, and Fig. 10 a crystal that, with the exception of a few spikes, is a single-domain with the polar axis lying in the crystal plane.

4. Pressed Disks

In order to measure absorption spectra without preparing thin single crystals, pressed disk samples of several materials were made by the technique of Stimson[20] and Schiedt.[21] A small section of a single crystal was powdered to a particle size of about one micron, and a few milligrams of the powder mixed with about 0.8 g of powdered KBr and then placed in a cylindrical die 20 mm in diameter. The die was evacuated to a pressure of 0.1 mm Hg.for 20 minutes to remove adsorbed water vapor, and the sample then pressed for 10 minutes at 30 tons/inch^2 in a hydraulic press.

Clear disks thus obtained could be used to about 300 cm^{-1}. These disks had a transmission in the region of an absorption band equivalent to that of a single crystal about 1 micron in thickness.

Fig. 9. A polarized light photomicrograph of a single crystal of $BaTiO_3$, 1.5 μ in thickness and about 1x2 mm in area, prepared by etching in phosphoric acid. This crystal exhibits a typical mixed-domain pattern.

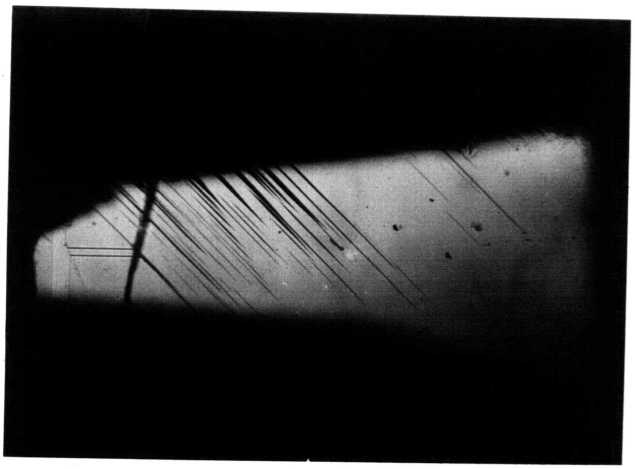

Fig. 10. A polarized light photomicrograph of a single crystal of $BaTiO_3$, 1.5 μ in thickness, and about 1x2 mm in area, prepared by etching in phosphoric acid. With the exception of the spiked domains, this crystal is single domain, with the polar axis lying in the crystal plane.

CHAPTER III

EXPERIMENTAL RESULTS

1. Thick Single-Crystal Measurements

In order to determine the general features of the absorption spectrum of $BaTiO_3$, initial measurements were made at room temperature on single crystals about 0.3 mm thick. A typical spectrum, similar to that observed by Hilsum[7], is shown in Fig. 11. Between 1 and 6 μ, the transmission has the practically constant value of about 70%, with the losses due almost entirely to reflection (n = 2.4). At shorter wavelengths, the transmission drops sharply as the electronic absorption edge at about 0.42 μ is approached. An absorption band sets in at about 6 μ, and complete cutoff is reached at about 10.5 μ. A shoulder at about 6.8 μ and a band at 8.1 μ can be discerned, due to impurities or to overtone or combination bands of lower frequency vibrations.

2. Pressed Disk Measurements

In the range from 1000 cm^{-1} to 300 cm^{-1} (10 to 33 microns), the transmission of these thick single crystals was extremely low; the absorption spectrum was therefore measured on powdered samples dispersed in pressed KBr disks, prepared as described previously. In the spectrum of Fig. 12, the weight of the powder sample corresponds to that of a single crystal 0.9 microns in thickness.

Two absorption bands are observed. The higher frequency band, between about 800 cm^{-1} and 475 cm^{-1}, is centered at 540 cm^{-1}. This band is assymetric, with a high frequency tail, and has a half width of about

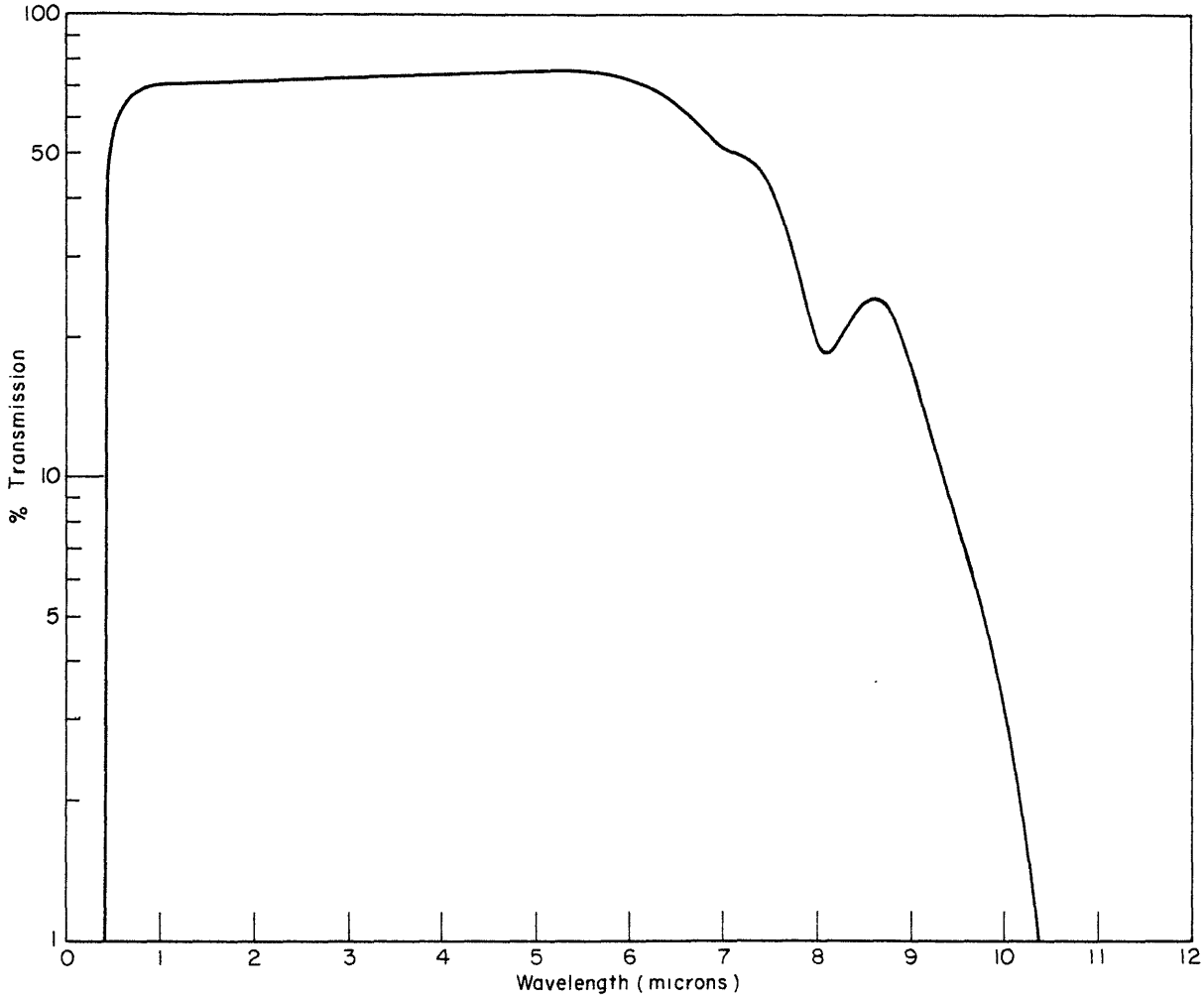

Fig. 11. Absorption spectrum of single crystal $BaTiO_3$, 0.26 mm in thickness.

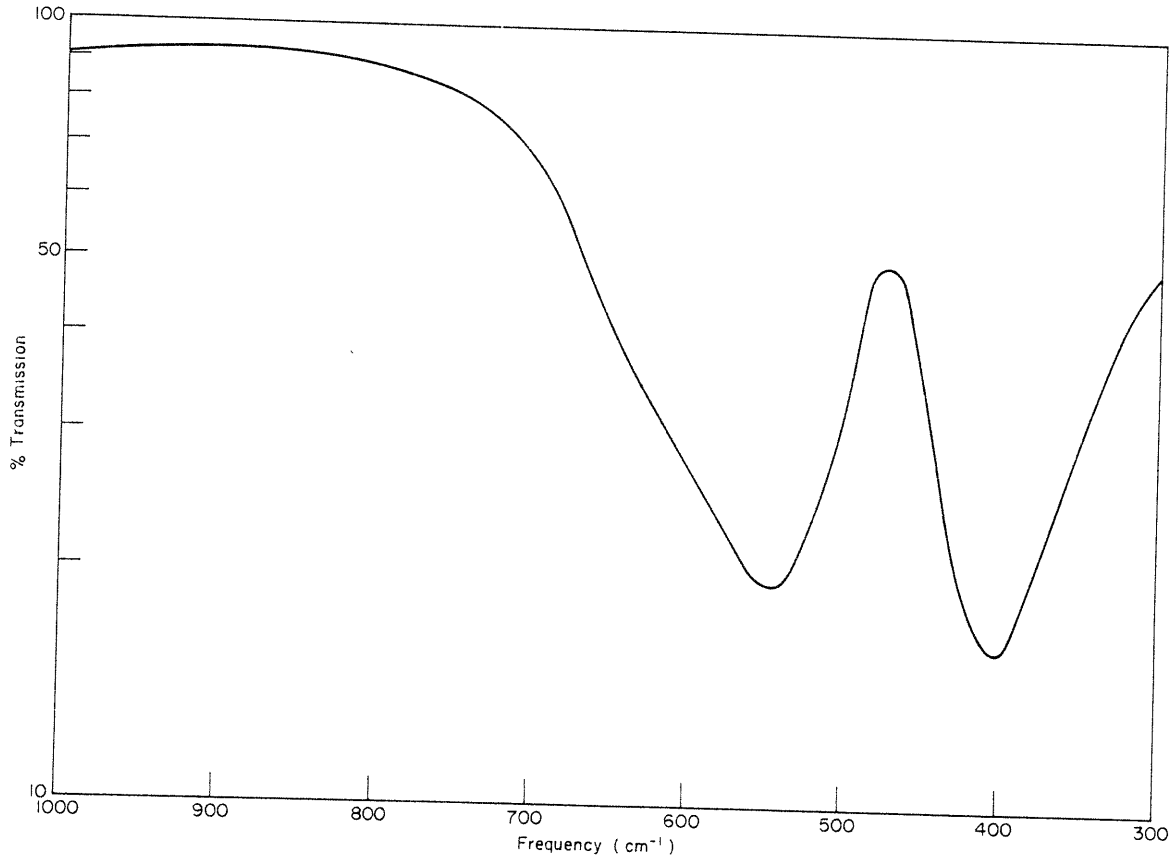
100
50
10
% Transmission
1000
900
800
700
600
500
400
300
Frequency (cm⁻¹)

165 cm^{-1}. The lower frequency band extends from about 475 cm^{-1} to the limit of the available experimental range at about 300 cm^{-1}, with a center at 400 cm^{-1} and a half width of about 120 cm^{-1}.

KBr prisms were used from the visible to about 425 cm^{-1}, and replaced by a KRS-5 prism for the region from 500 cm^{-1} to 300 cm^{-1}. The point of exchange occured conveniently at the "transmission window" between the two bands. The agreement in the overlap region covered by both prisms was excellent.

The spectrum of the pressed disk sample as a function of temperature for the 540 cm^{-1} band is shown in Fig. 13. No difference was observed here in the spectra of the cubic and tetragonal phases of $BaTiO_3$. In the orthorhombic phase, a shoulder develops at about 505 cm^{-1}, and the band center shifts to slightly higher frequency. In the rhombohedral phase, bands are observed at 500 cm^{-1} and 550 cm^{-1}. No significant difference was observed in the four phases for the 400 cm^{-1} band.

3. Thin Single-Crystal Absorption Measurements

Pressed disk samples have the disadvantage that the phase transitions are very sluggish for the fine powders used, and the spectra therefore may represent those of mixed phases. Also, since the particles are oriented at random in the disk, it is not possible to measure in different crystallographic directions. Thin single crystals, etched to a thickness of about 1.5 microns, were therefore investigated in the variable temperature microcell previously described. The measurements could only be extended from the visible to about 400 cm^{-1}, due to the lack of sufficient radiant energy in the far infrared, therefore restricting measurements to the higher of

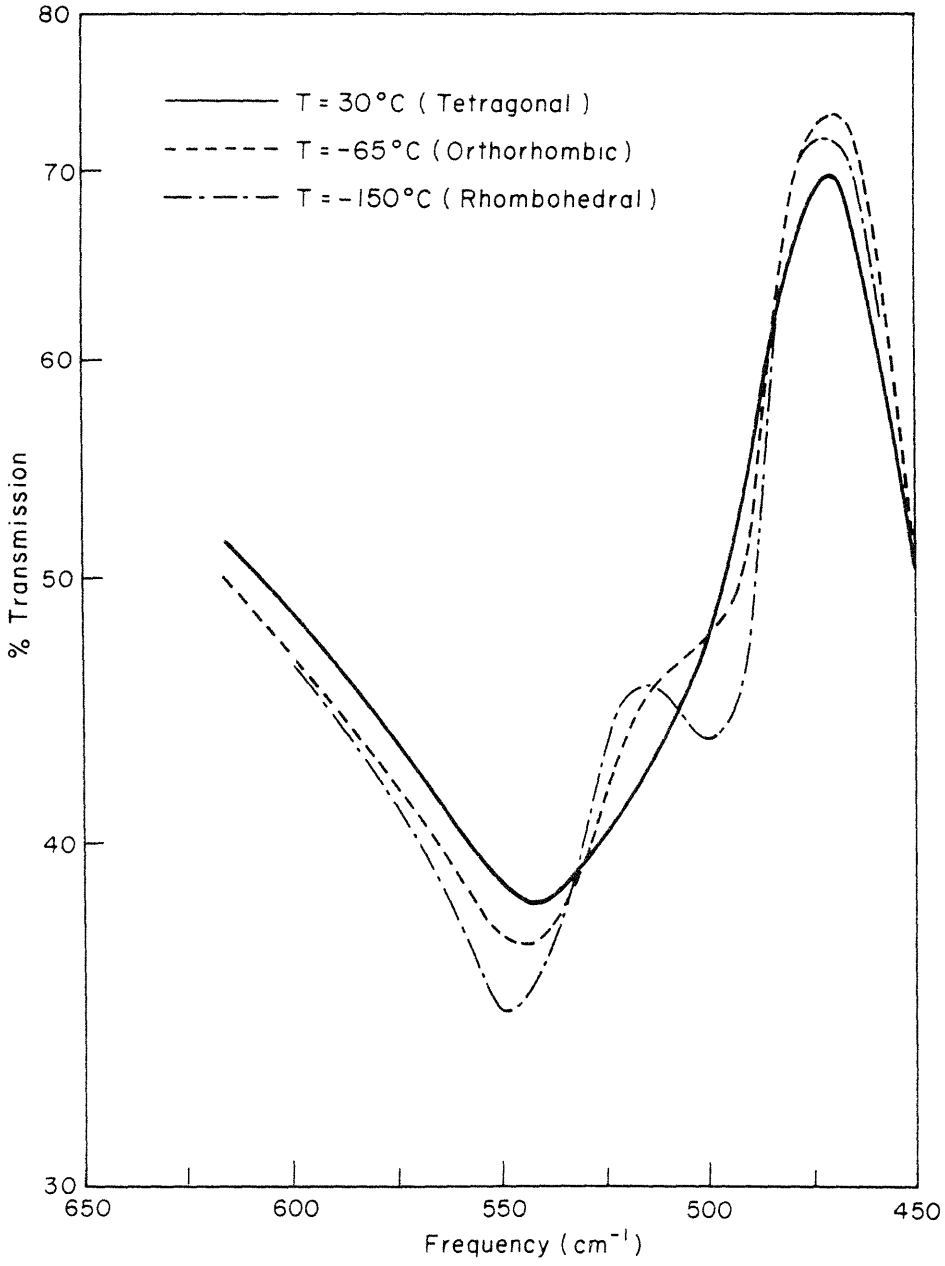

Fig. 13. Low temperature absorption spectra of powder $BaTiO_3$

the two absorption bands observed in the pressed disk spectra.

Room-temperature measurements were carried out to observe the difference in vibrational frequency along the polar axis (the "c" direction) and at right angles to this axis (the "a" direction), using a single-domain "a" plate, with the polar axis in the crystal plane. The "a" and "c" directions were established with a quartz wedge and polarizing microscope. As a photomicrograph of the crystal shows (Fig. 10), a few spiked domains with the "c" axis normal to the crystal plane remained and comprised about 5% of the crystal surface. Therefore, the observed "c" spectrum contains about 5% "a" spectrum.

The spectra measured using polarized infrared radiation (AgCl sheet polarizer) are shown in Fig. 14. The "a" spectrum is centered at 495 cm^{-1}, and the "c" spectrum at 517 cm^{-1}. The "c" band is somewhat broader, due in part to the presence of the spiked domains. The intensities of the two bands are approximately equal.

Measurements were also made with unpolarized radiation on several mixed-domain crystals, and on crystals which had the "c" axis normal to the crystal face ("c" plate). For the "c" plate crystal, the band center was located at 495 cm^{-1}, since only vibrations along the "a" axis are excited. For a mixed-domain plate, the band center lay between 495 cm^{-1} and about 510 cm^{-1}, depending on the particular way in which the domains were arranged.

The spectrum, measured at elevated temperatures using hot oil in the microcell temperature reservoir, remained unchanged from room temperature to the Curie point. Above the Curie point, the band was centered at 495 cm^{-1}, as shown in Fig. 15.

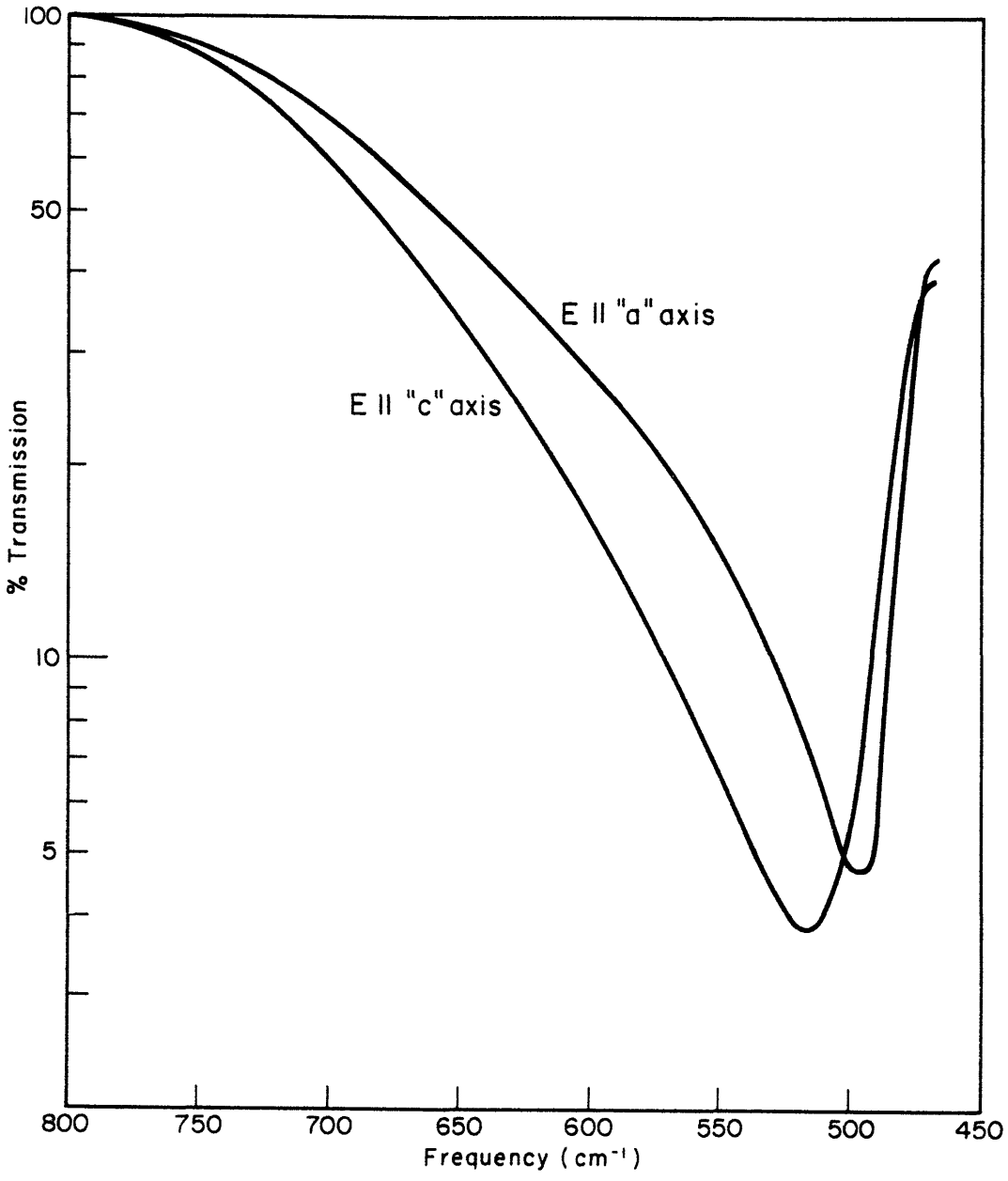

Fig. 14. The polarized infrared absorption spectra of tetragonal single crystal $BaTiO_3$, 1.5 μ in thickness, along the "c" and "a" axes.

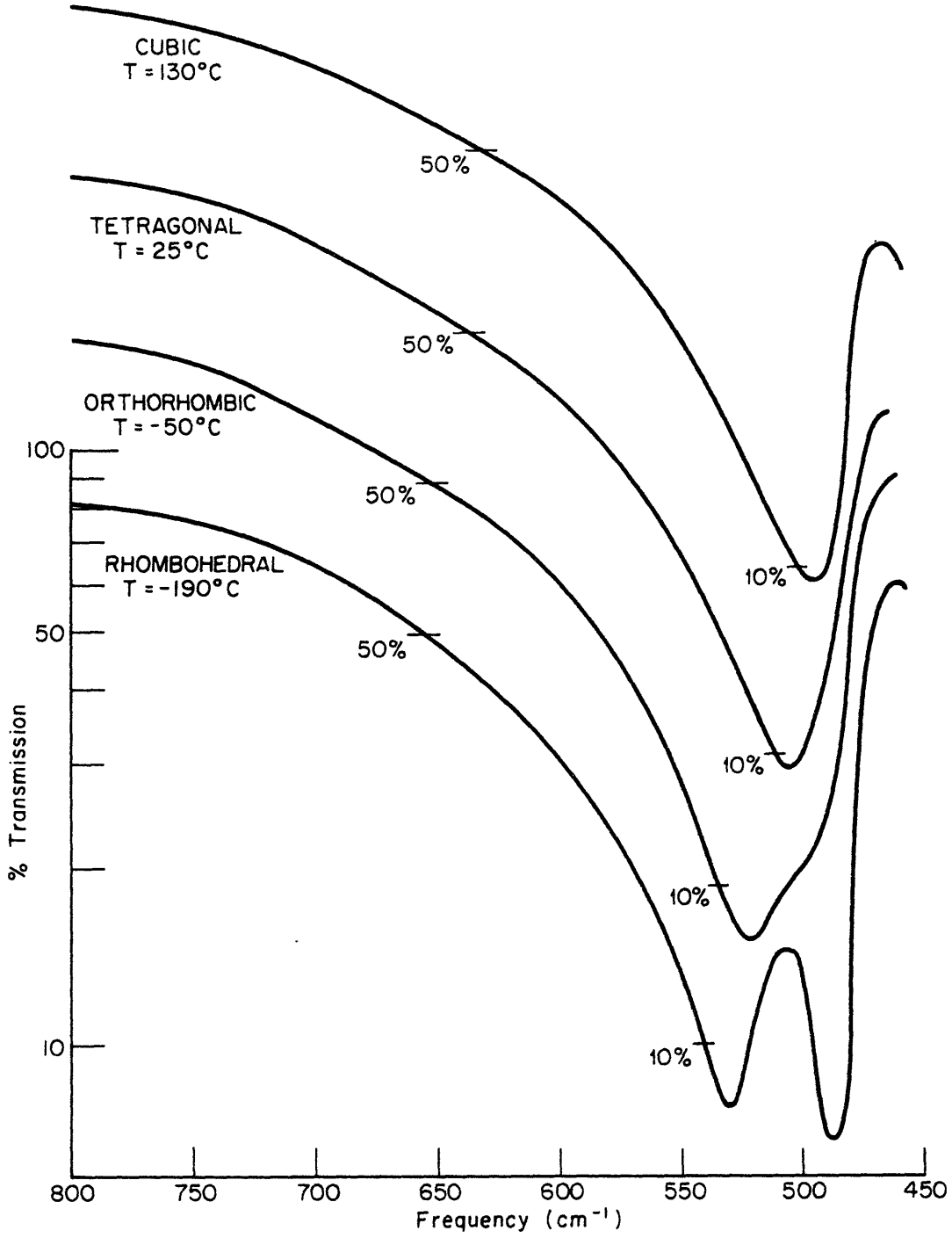

Fig. 15. The infrared absorption spectra of single crystal $BaTiO_3$, 1.5 μ in thickness, for the cubic, tetragonal, orthorhombic, and rhombohedral phases.

In order to observe any possible absorption anomalies at temperatures in the immediate vicinity of the Curie point, the monochromator was set on a point near the band center and the temperature raised slowly through the Curie point. Aside from the slight intensity jump caused by the shift of the band center at the Curie point, no intensity change was observed for an "a" plate or for a mixed-domain crystal. For the case of a "c" plate, where the vibrational frequency was the same above and below the Curie point, no intensity jump was recorded.

Low-temperature measurements (Fig. 15) were made in the temperature region from 25°C to -70°C, with dry ice and methanol in the microcell reservoir, and from -70°C to -190°C, with liquid nitrogen. Good thermal contact between the reservoir and the crystal was assured by fastening the crystal to a KBr plate with a layer of vaseline, so thin that it did not absorb in this special region. The KBr plate was fastened to a sample holder in thermal contact with the temperature reservoir, and the crystal temperature measured by a thermocouple imbedded in the KBr plate.

In the orthorhombic phase, the band is centered at 520 cm^{-1}, with a shoulder at 495 cm^{-1}. In the rhombohedral phase, it splits into two bands, located at 530 cm^{-1} and 490 cm^{-1}. The band shape in the vicinity of the band center is shown in Fig. 16, and the location of the band centers as a function of temperature in Fig. 17. The transition between the orthorhombic and rhombohedral phases covers a temperature range of about 30°C. Within a given phase, the ratio of the band intensities changes with temperature, but the position of the band centers remains constant.

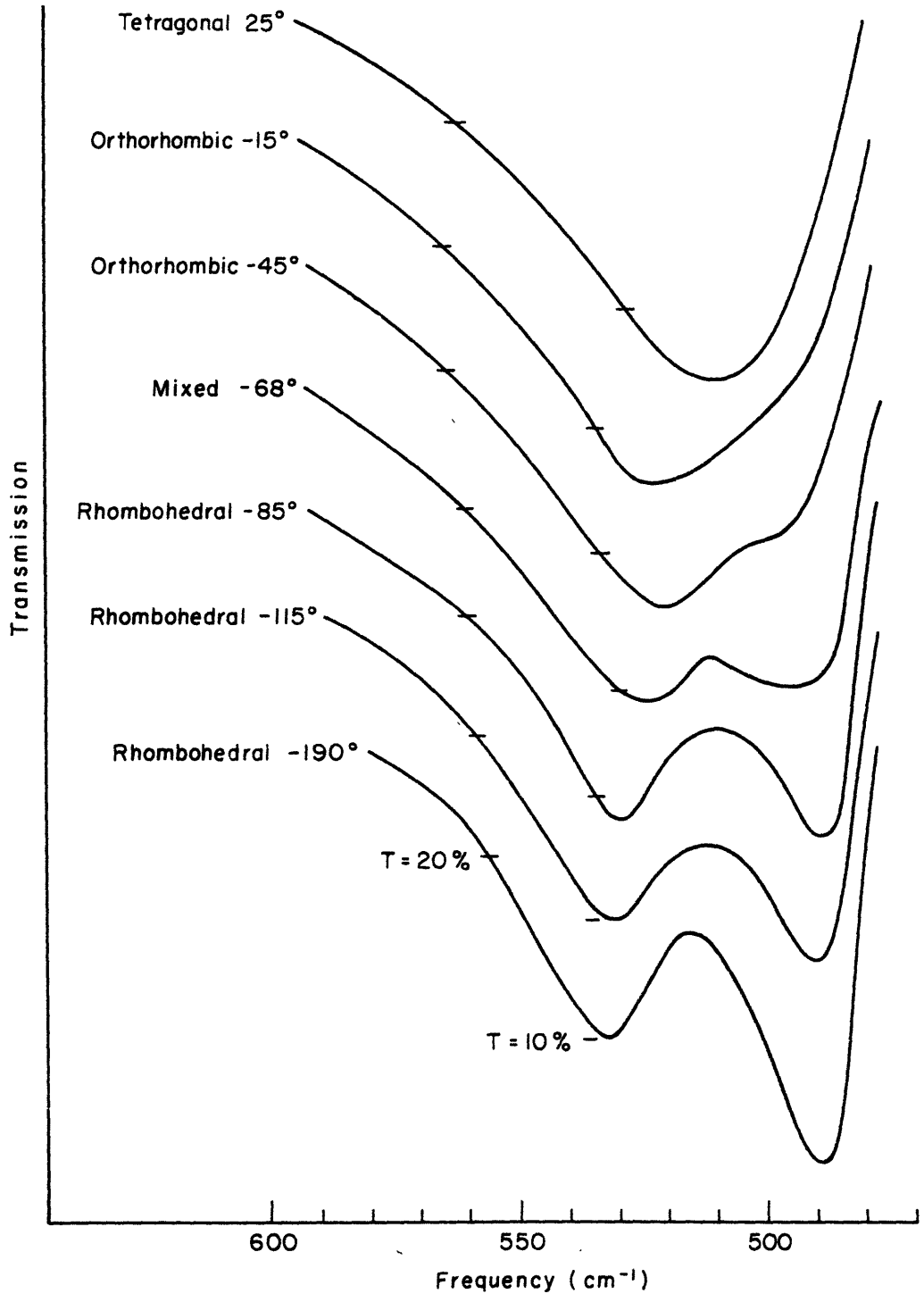

Fig. 16. Details of the infrared absorption band center in single crystal $BaTiO_3$, 1.5 μ in thickness, at low temperatures.

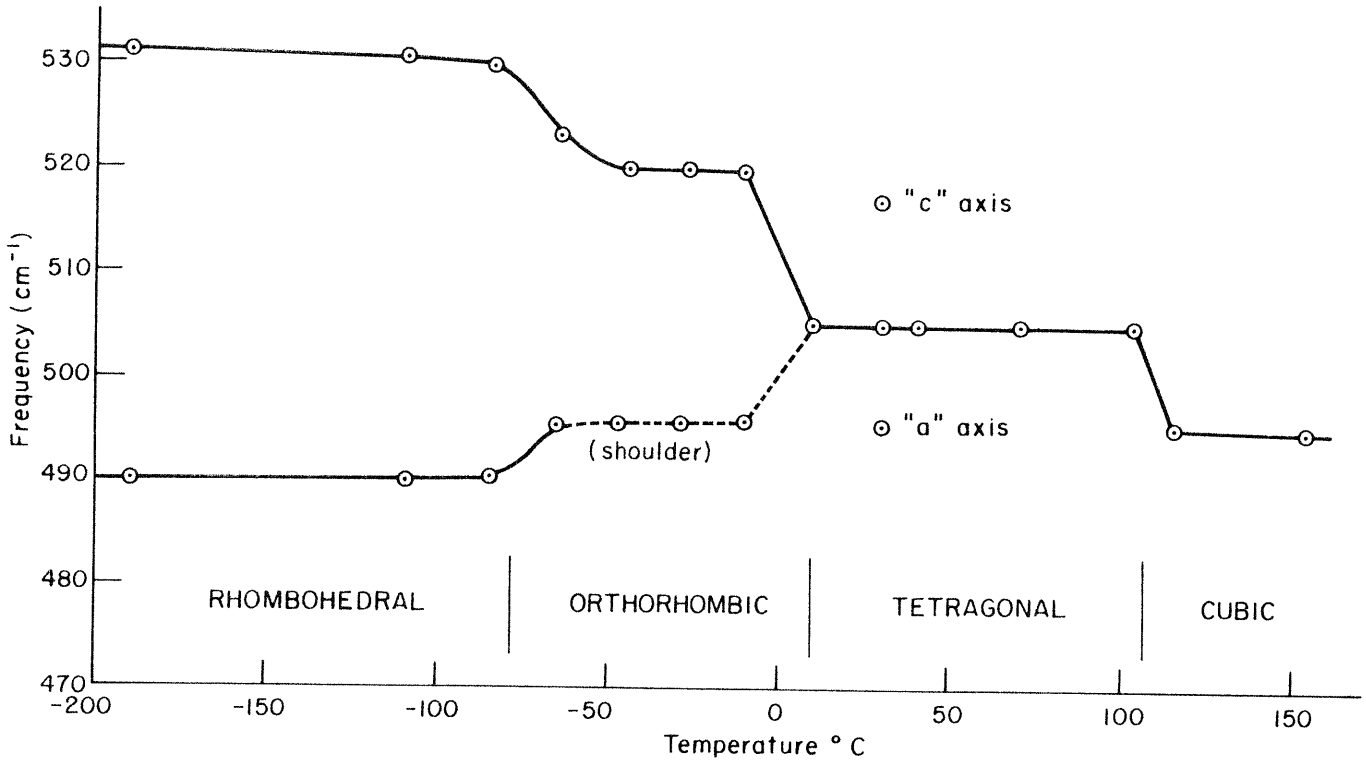

Fig. 17. Location of the infrared absorption band center for single crystal $BaTiO_3$ as a function of temperature. (In the tetragonal phase, "a" and "c" band centers are shown in addition to the unpolarized light measurements).

4. Reflection Measurements

The reflection spectra of single crystals of $BaTiO_3$ were measured from the visible to 400 cm^{-1}, with the reflection device shown in Fig. 3. The spectrum at approximately normal incidence for a mixed-domain crystal is shown in Fig. 18. A broad band, centered at a somewhat higher frequency than the absorption band, is observed. The crystal reflectivity drops to zero at 800 cm^{-1}, the point where the index of refraction is unity, and rises slowly at higher frequencies. A narrow region of low reflectivity is observed at 475 cm^{-1}, corresponding to the "transmission window" in the absorption spectrum. At the lowest frequencies measured the reflectivity is very high.

Reflection measurements were also made on a single-domain plate with the polar axis normal to the crystal face ("c" plate), prepared by cooling a crystal through the Curie point under a transverse electric field. No differences were observed between this spectrum and that of the multi-domain crystal.

While the general shape of the reflectivity curve is correct, the absolute intensity may be in error by as much as 10%, due to the difficulty of positioning the sample in exactly the same position as the masked area of a standard mirror, and to the low incident light intensity resulting in a low signal to noise ratio.

5. Hexagonal $BaTiO_3$

In addition to the perovskite modification of $BaTiO_3$, where the TiO_6 octahedra are joined at corners, a hexagonal modification exists,

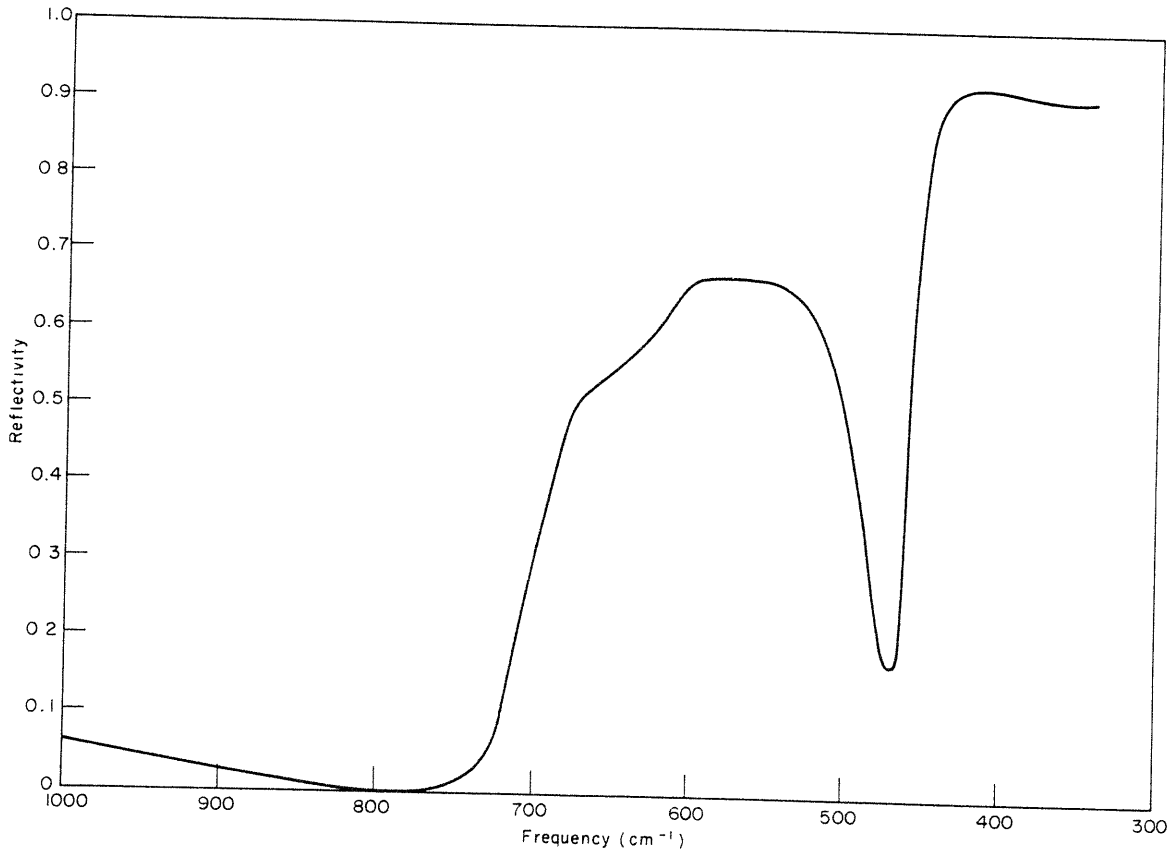
1.0
0.9
0.8
0.7
0.6
0.5
0.4
0.3
0.2
0.1
0
Reflectivity
1000
900
800
700
600
500
400
300
Frequency (cm⁻¹)

where two-thirds of the octahedra occur in pairs which share a face to form Ti_2O_9 co-ordination groups.[22] This modification is not ferroelectric, and no phase transitions have been reported.

The absorption spectrum of a pressed disk sample prepared from a boule of hexagonal $BaTiO_3$ grown by J. Smiltens in this laboratory is shown in Fig. 19. The spectrum was measured at 25°C and at -150°C. The high frequency band, centered at 555 cm^{-1}, lies slightly higher than the corresponding band in perovskite $BaTiO_3$; its half width is about 200 cm^{-1}, about 40 cm^{-1} wider than the perovskite band. The low-frequency band, centered at 360 cm^{-1}, about 40 cm^{-1} lower than the perovskite low-frequency band, shows evidence of fine structure.

Apart from some sharpening of the absorption band at low temperatures, no difference between the room temperature and low temperature spectra occurs, in contrast to the difference found for the perovskite modification.

6. Effect of Cation Replacement

The spectra of several titanates related to $BaTiO_3$ by cation replacement were investigated: the perovskite titanates $PbTiO_3$, $SrTiO_3$, and $CaTiO_3$, which are tetragonal, cubic, and orthorhombic, respectively, at room temperature, and the ilmenite titanates $CdTiO_3$, $ZnTiO_3$, and $MgTiO_3$.

Small single crystals of $PbTiO_3$, obtained from the Bell Telephone Laboratories, were etched to a thickness suitable for transmission measurements by the techniques employed for $BaTiO_3$. The high Curie temperature of $PbTiO_3$ necessitated etching the crystals in the tetragonal

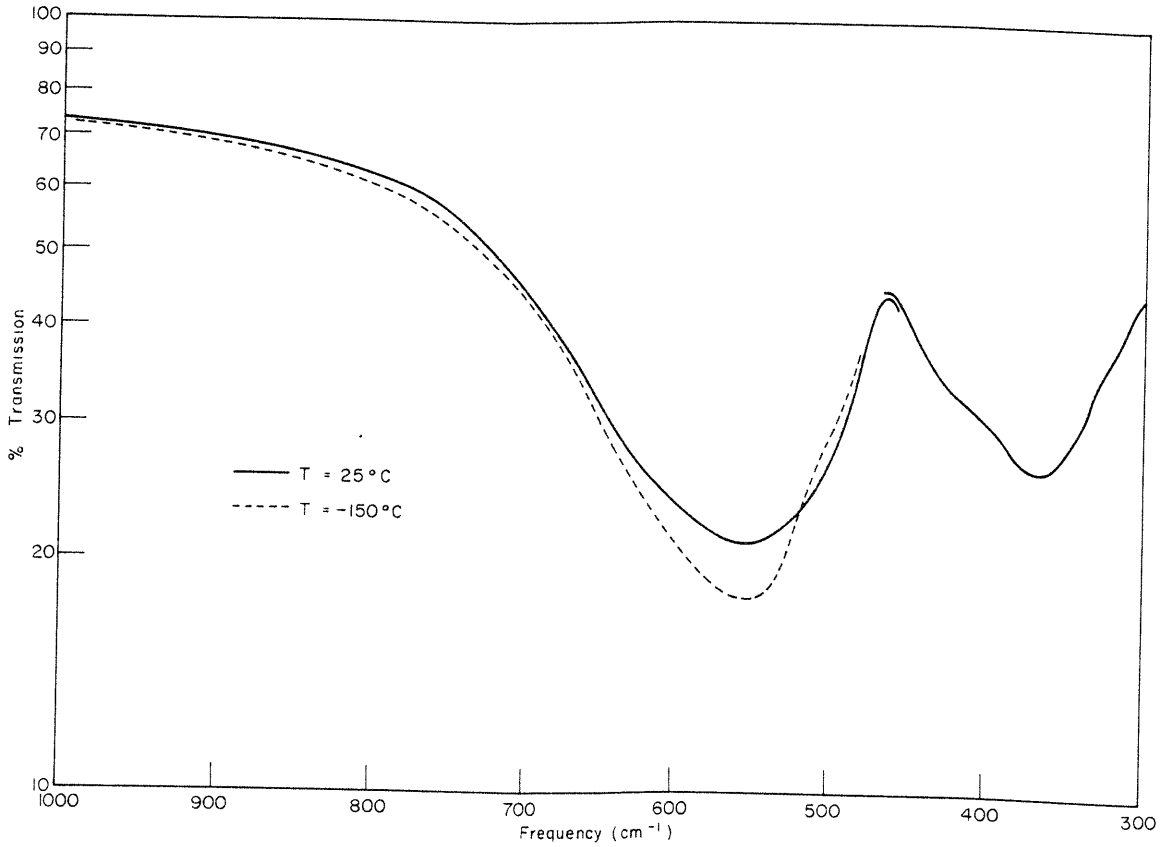
100
90
80
70
60
50
40
30
20
10
% Transmission
T = 25°C
T = -150°C
1000
900
800
700
600
500
400
300
Frequency (cm⁻¹)

Fig. 12. [illegible]

phase; some selective domain etching resulted. Another complicating factor was the presence of PbO inclusions which etched more quickly than the crystal itself, which ultimately caused holes to appear. A crystal was finally obtained about 2 microns in thickness which had about 90% of the crystal area intact in the masked section used for the absorption measurements. The absorption spectrum of this crystal, corrected for the presence of light transmitted through the holes, is shown in Fig. 20. The absorption band is centered at 535 cm^{-1}, and has a shoulder at about 610 cm^{-1}. The crystal was too fragile to allow the measurement of the spectrum at low temperatures.

The spectrum of a powdered sample of $PbTiO_3$ dispersed in a pressed KBr disk was measured at 25°C and -190°C. Bands were observed at 590 cm^{-1} and 405 cm^{-1}, which sharpened slightly but did not split at low temperatures. The reflection spectrum of a single crystal showed a broad reflection band similar to that of $BaTiO_3$.

Since unreacted PbO was present in the crystals, a pressed disk spectrum of PbO was measured in the region between 1000 cm^{-1} and 300 cm^{-1}. No absorption bands were found.

A boule of $SrTiO_3$ grown by the flame fusion process was obtained from the National Lead Company. A small section of the boule was powdered and the pressed disk spectrum measured. Bands were observed at 610 cm^{-1} and 395 cm^{-1}, which did not sharpen appreciably at low temperatures. The reflection spectrum of the polished face of the boule was found to be similar to that of the other perovskite titanates.

The absorption spectra of pressed disks and the reflection spectra of single crystals of $PbTiO_3$ and $SrTiO_3$ are shown in Figs. 21 and 22,

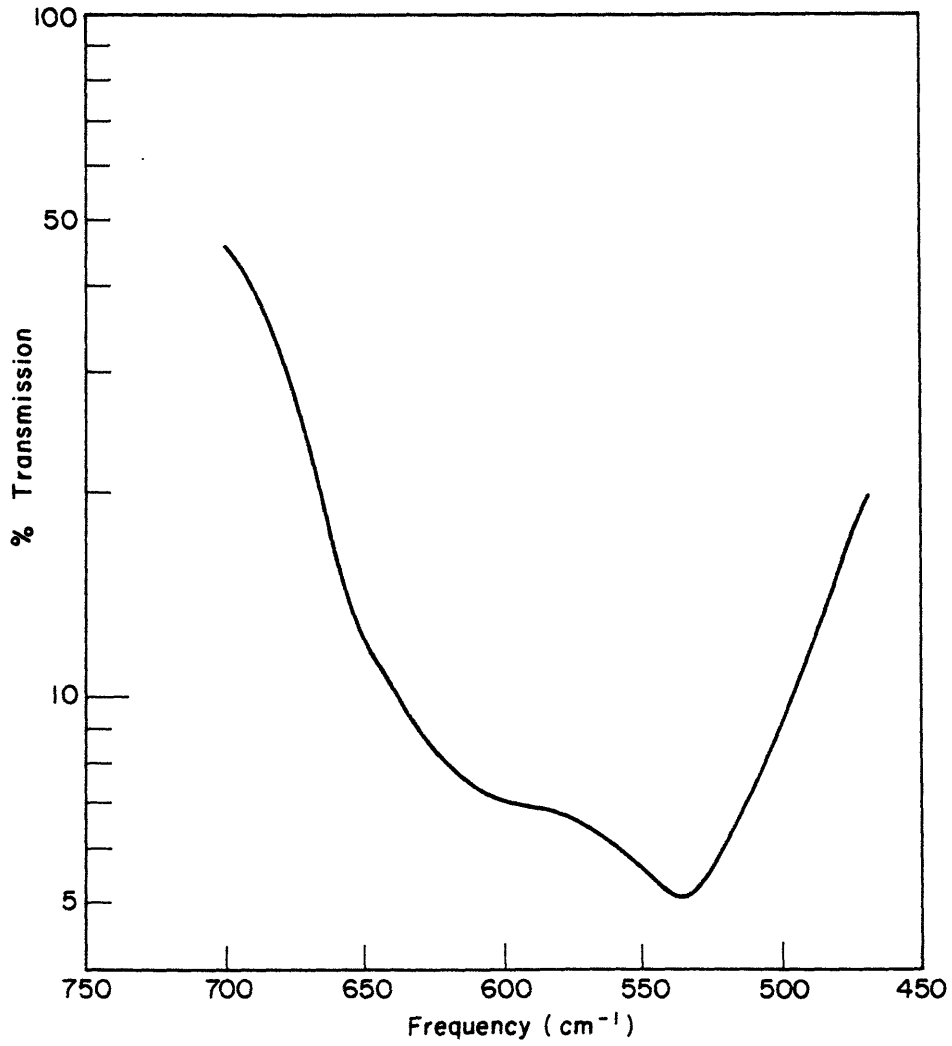

Fig. 20. Absorption spectrum of single crystal $PbTiO_3$, 2 μ in thickness.

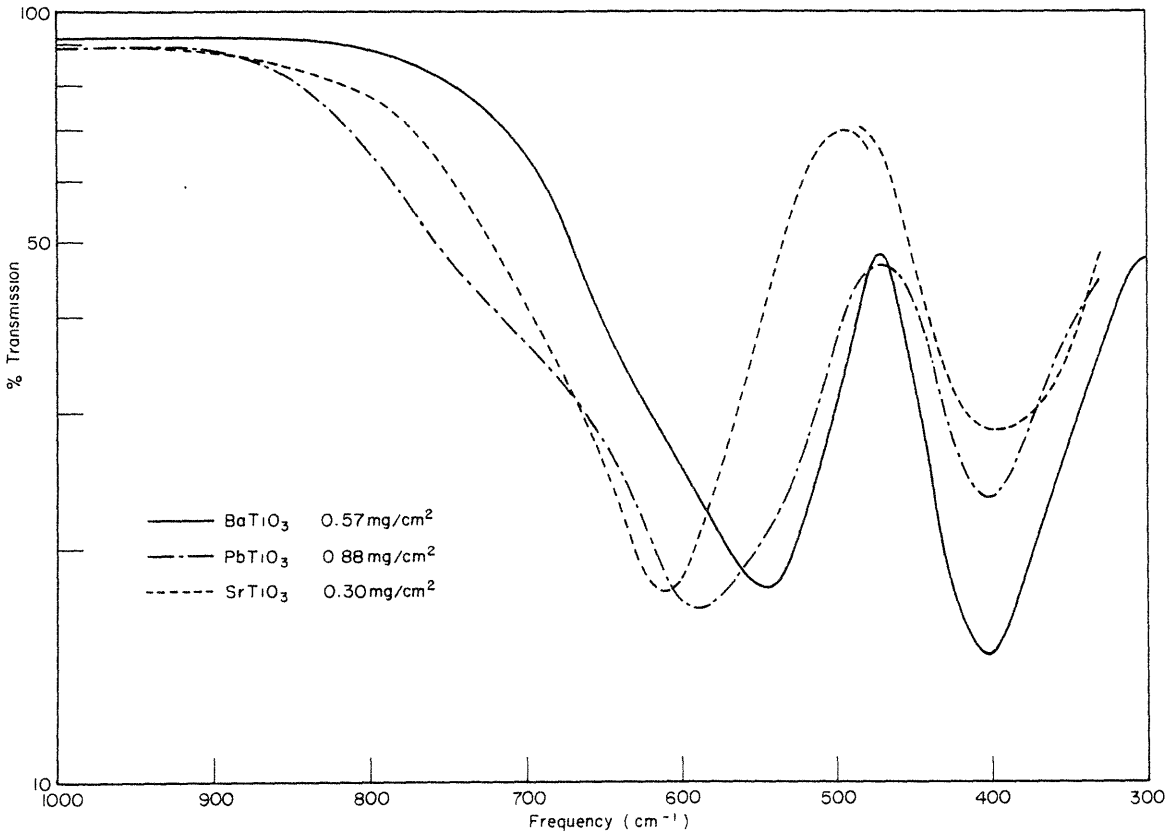

Fig. [illegible] Infrared absorption spectra of powder $BaTiO_3$, $PbTiO_3$ and $SrTiO_3$

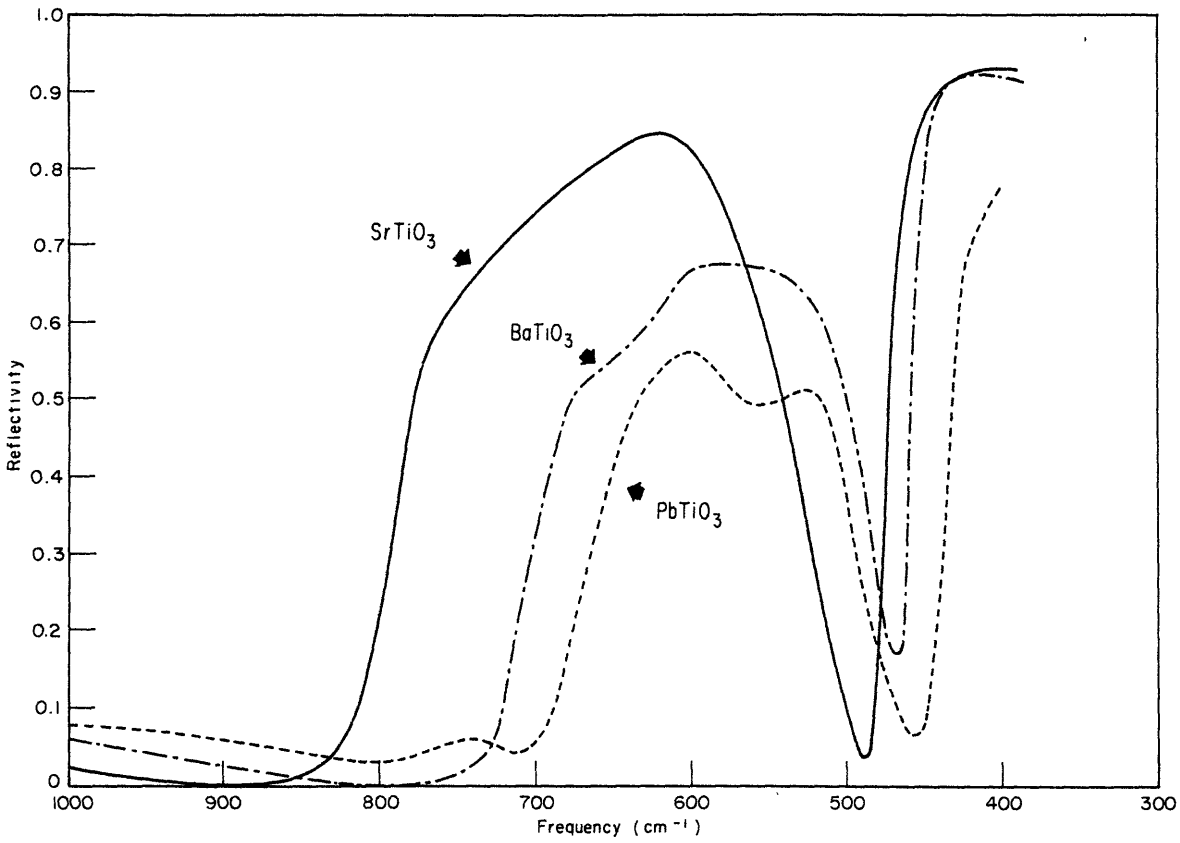

Fig. 22. The infrared reflection spectrum of single crystal $BaTiO_3$, $SrTiO_3$, and $PbTiO_3$.

together with corresponding spectra of $BaTiO_3$.

Samples of $CaTiO_3$, $CdTiO_3$, $ZnTiO_3$, and $MgTiO_3$, obtained in the form of powders from the National Lead Company, give the absorption spectra of Figs. 23 and 24. The spectrum of $CaTiO_3$ has the same general features as that of $BaTiO_3$; fine structure appears, caused by the lower symmetry of this material and by the presence of unreacted material in the powder used. In the three ilmenite titanates $CdTiO_3$, $ZnTiO_3$, and $MgTiO_3$, the high-frequency band is much broader than in $BaTiO_3$, and the low-frequency band is doubled.

The location of the band centers of all materials measured in this investigation are listed in Table III.

7. $KNbO_3$ and $NaNbO_3$

$KNbO_3$ and $NaNbO_3$ of a perovskite form similar to $BaTiO_3$, have high temperature Curie points((410°C and 640°C, respectively), several high temperature transitions, and are orthorhombic at room temperature.[23-25] $KNbO_3$ is ferroelectric at room temperature, and has a transition to a rhombohedral phase at about -50°C, showing pronounced thermal hysteresis. $NaNbO_3$, antiferroelectric at room temperature, has a transition to a ferroelectric state at about -200°C, again with a large thermal hysteresis.

Pressed powder disks of $KNbO_3$ and $NaNbO_3$ were prepared from powdered crystal sections of single crystals obtained from the Bell Telephone Laboratories. The spectra (Fig. 25) are similar to that of orthorhombic $BaTiO_3$, with a shoulder on the low-frequency side of the higher frequency band. The band centers in $KNbO_3$ are located at 660 cm^{-1}, 550 cm^{-1} (shoulder), and 375 cm^{-1}; in $NaNbO_3$ at 675 cm^{-1}, 510 cm^{-1} (shoulder), and

Table III. Absorption Band Centers

Single Crystal Spectra

$BaTiO_3$	(cubic)	495 cm^{-1}
"	(tetragonal)	517; 495
"	(orthorhombic)	520; 495 (shoulder)
"	(rhombohedral)	532; 490
$PbTiO_3$	(tetragonal)	610 (shoulder); 535

Pressed Disk Spectra

$BaTiO_3$	(tetragonal)	545 cm^{-1}	400 cm^{-1}
"	(hexagonal)	555	365
$PbTiO_3$	(tetragonal)	590	405
$SrTiO_3$	(cubic)	610	395
$CaTiO_3$	(orthorhombic)	540; 700 (shoulder)	360 (broad)
$KnBO_3$	(orthorhombic)	660; 550 (shoulder)	375
$NaNbO_3$	(orthorhombic)	675; 510 (shoulder)	375
$CdTiO_3$	(ilmenite)	575 (broad)	425; 335
$ZnTiO_3$	(ilmenite)	590 (broad)	400; 315 (shoulder)
$MgTiO_3$	(ilmenite)	600 (broad)	475; 350

375 cm^{-1}. Little difference was observed between the room temperature and low temperature spectra.

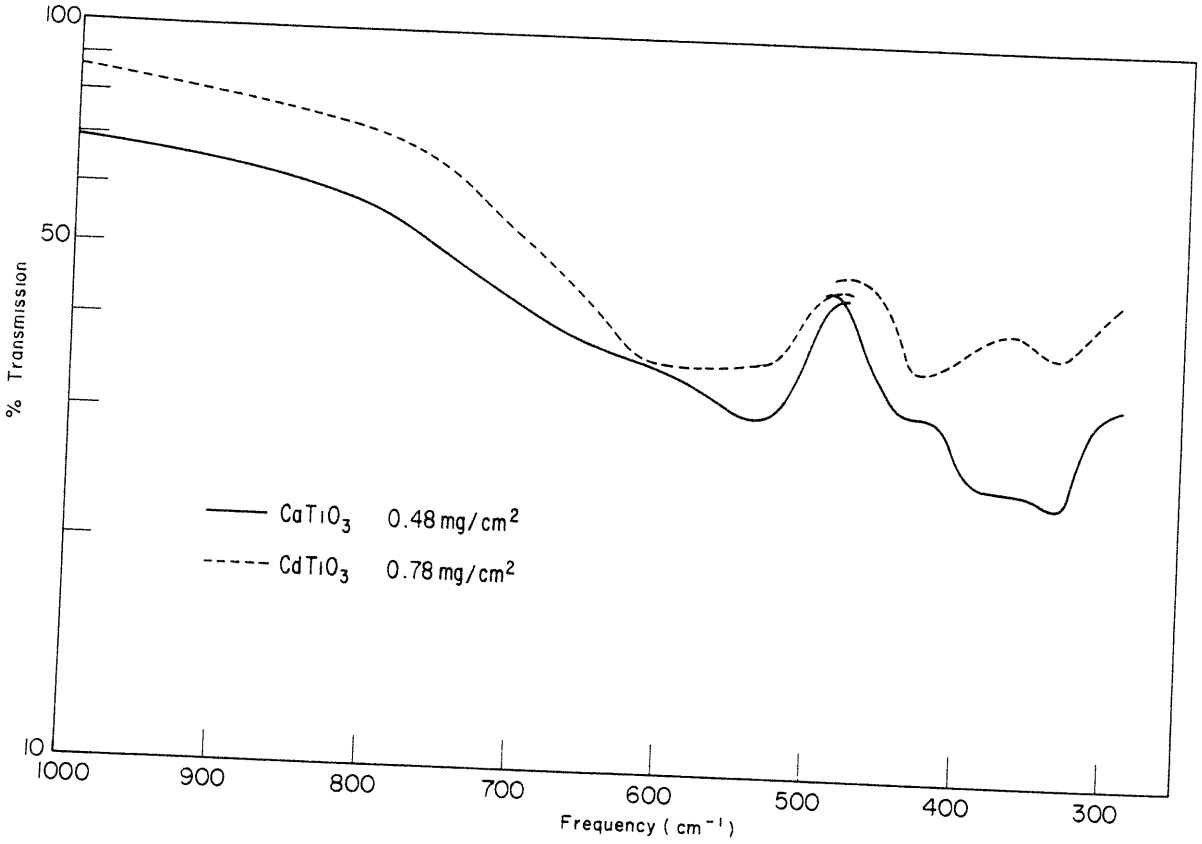

Fig. 23. The infrared absorption spectra of powder [illegible]

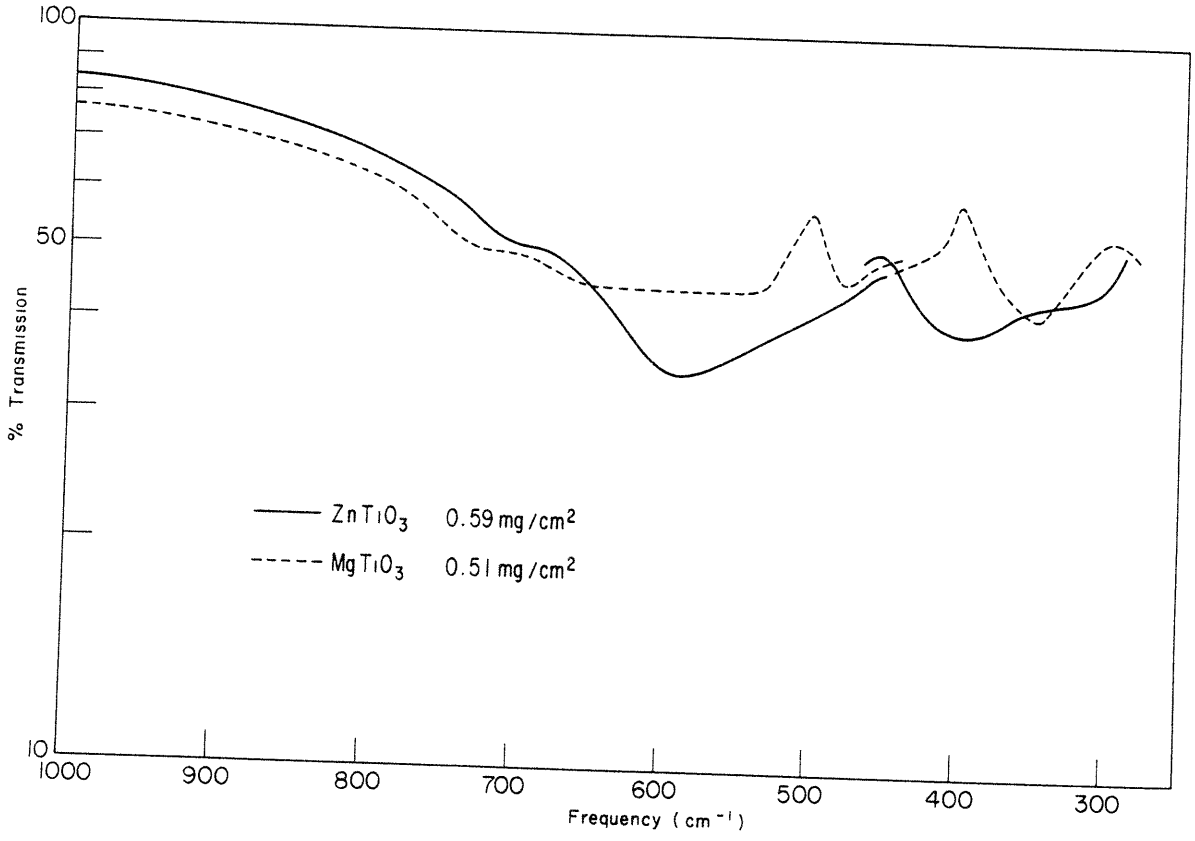
100
50
10
% Transmission
ZnTiO3 0.59 mg/cm2
MgTiO3 0.51 mg/cm2
1000
900
800
700
600
500
400
300
Frequency (cm-1)

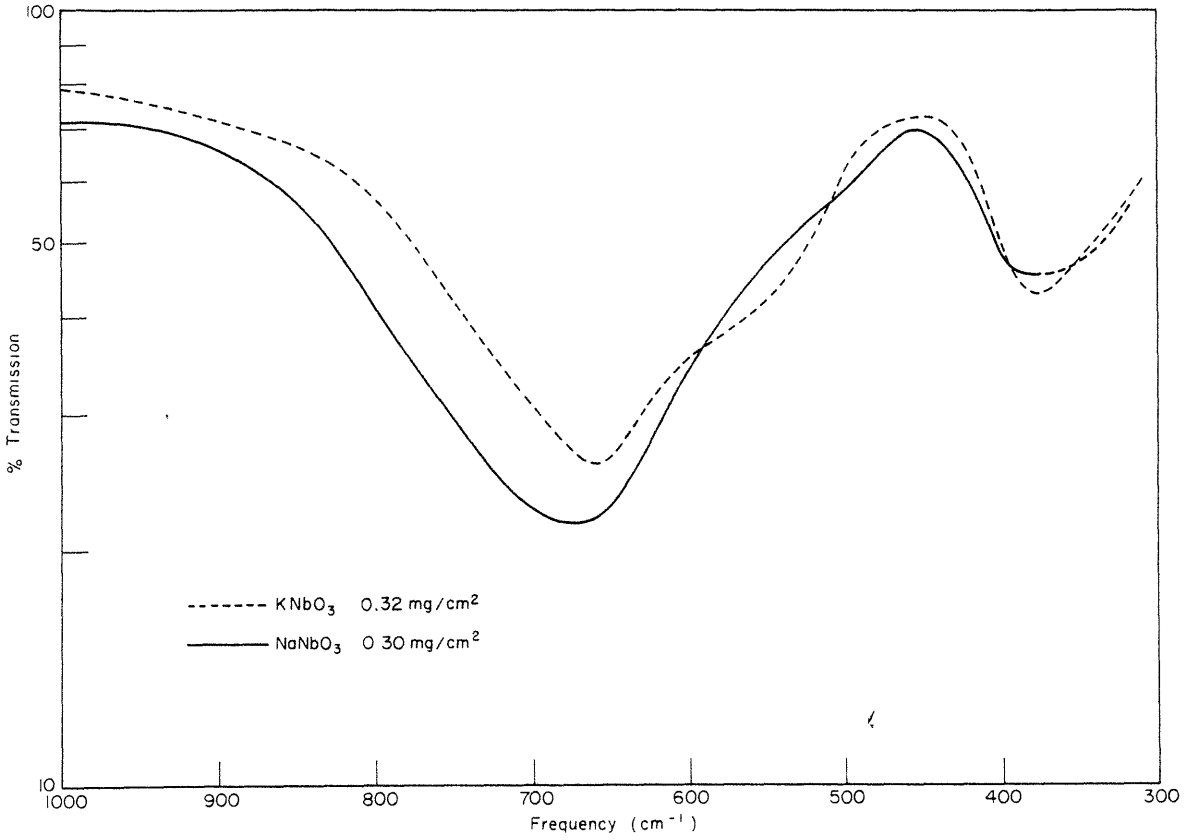

Fig. 15. The infrared absorption spectra of powder $KNbO_3$ and $NaNbO_3$.

8. Effect of Added Iron

The perovskite $BaTiO_3$ crystals used in this investigation were grown from a KF flux, by a variation of the technique described by Remeika.[26] About 0.2% Fe_2O_3 is ordinarily added to the melt to aid in the formation of large single-domain crystals and to reduce the dielectric loss. The addition of this amount of iron oxide lowers the Curie point by about 10°C, and decreases the c/a ratio slightly.

The effect of added iron on the infrared spectrum of $BaTiO_3$ was investigated. Four pressed disk samples were measured, prepared from crystals with Fe_2O_3 addition ranging from zero to 0.4%. No differences were observed in band intensity or location.

9. Effect of Disk Matrix Material

In order to investigate the dependence of the shape and location of the absorption spectrum of powdered $BaTiO_3$ on the optical properties of the material in which it is dispersed, identical $BaTiO_3$ samples were dispersed in matrices of increasing indices of refraction: KBr, AgCl, TlCl, and TlBr.

The centers of the absorption bands shift to lower frequencies when higher index materials are used (Table IV).

Table IV. Powder Absorption Band Centers in $BaTiO_3$.

Disk Material	Index of refraction (540 cm^{-1})	Absorption maxima	
KBr	1.48	545 cm^{-1};	400 cm^{-1}
AgCl	1.92	540	380
TlCl	2.06	532	365
TlBr	2.25	535	360

CHAPTER IV

DISCUSSION

1. Thin Crystal Transmission

The quantity of physical interest for a discussion of the spectrum of $BaTiO_3$ in terms of force constants and specific heats is the frequency of maximum absorption of the band. The use of both pressed disks and thin single crystal samples introduces complications in the determination of this absorption maximum.

The observed transmission curve of thin single crystals is a combination of beam attenuation effects due to crystal absorption and reflection from the crystal surfaces. Since the bands for maximum reflection occur at somewhat higher frequencies than for absorption, the true transmission minimum (or maximum absorption) will lie at somewhat lower frequencies than that observed in the uncorrected single crystal spectrum. An exact computation of the total reflectivity of the crystal, a function of the single surface reflectivity, the integrated angle of incidence, and interference between front and rear surface reflected beams, would require accurate values of the optical constants of the material and several geometrical parameters. Using available data on the transmission of the thin crystal, and the single surface reflectivity of a thick crystal, the limiting cases of constructive and destructive interference can be calculated and will serve to place limits on the frequency of the transmission minimum.

As shown in Appendix I, the fraction T of the beam transmitted through the body of the material can be expressed, in the vicinity of the transmission minimum, as:

$$T = \frac{D}{(1 - R)^2 \pm 2DR} \quad ,$$

where D is the observed transmission, R the single surface reflectivity, and the plus and minus signs used for the limiting cases of destructive and constructive interference. Figure 26 shows that the measured transmission minimum at 505 cm^{-1} is shifted to 495 cm^{-1} for the case of destructive interference and to 493 cm^{-1} for constructive interference. The true transmission curve will lie between these two curves. Although the intensities of the two corrected curves are greatly different, there is little change in the position of minimum transmission.

2. Pressed Disk Transmission

It has been observed in this investigation that the absorption band centers for the $BaTiO_3$ pressed disk samples shift to lower frequencies when the index of refraction, and thus the atomic polarizability, of the disk matrix is increased (Table IV). In Fig. 26A, the absorption band center for the higher frequency band ν_1 is plotted against the reciprocal of the index of refraction of the disk matrix material. The band center for the single crystal sample is included on this graph by considering the single crystal to consist of a powder dispersed in a matrix of $BaTiO_3$, and computing the impedance (= $1/n^*$) of the powder at the band center from reflectivity data.

For $BaTiO_3$, the high frequency band is centered at 545 cm^{-1} for the KBr pressed disk sample and at 495 cm^{-1} for the single crystal; for $PbTiO_3$, the only other material for which both single crystal and pressed disk

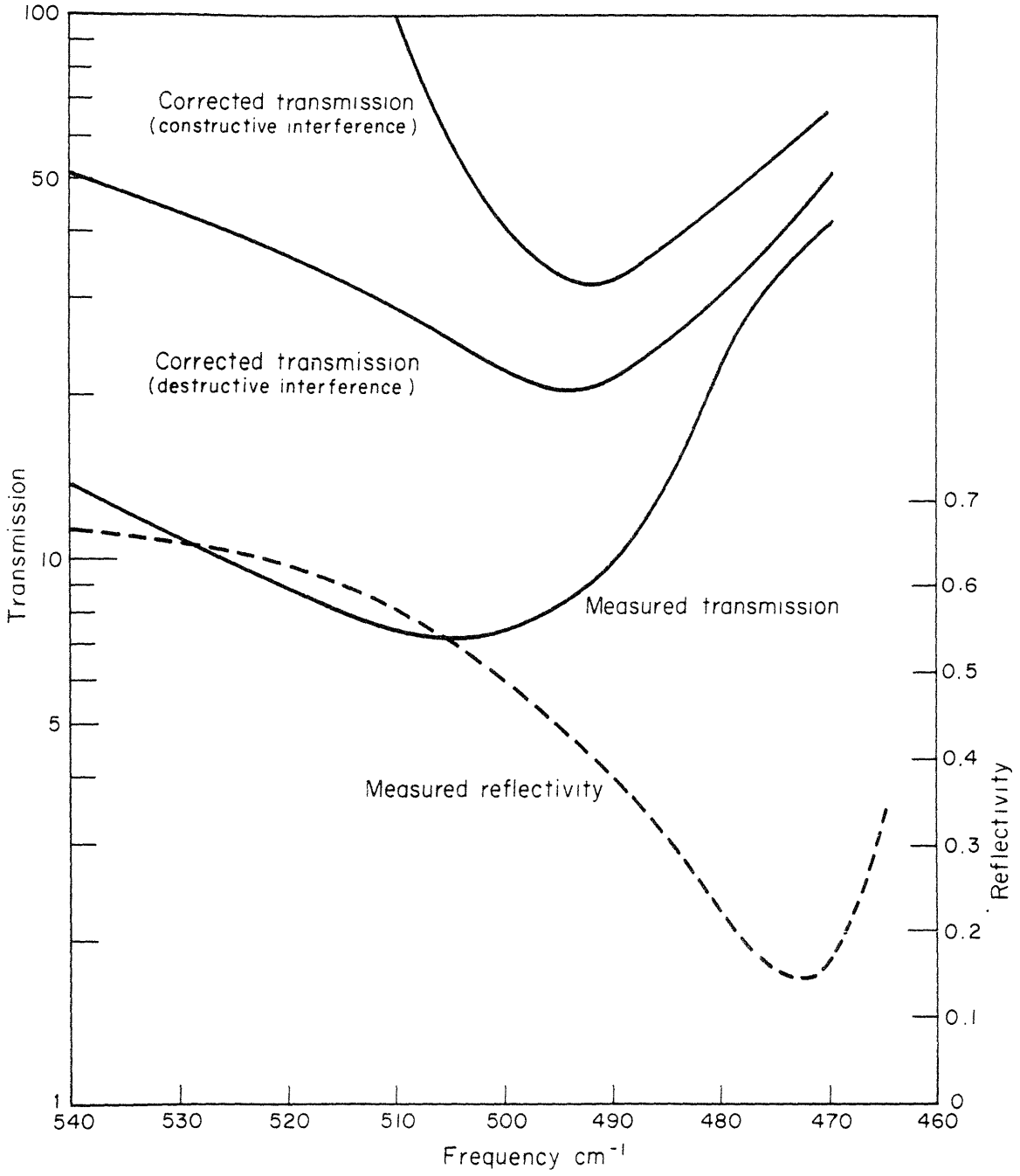

Fig. 26. Transmission of $BaTiO_3$ single crystal 1.5 μ in thickness, corrected for constructive and destructive interference.

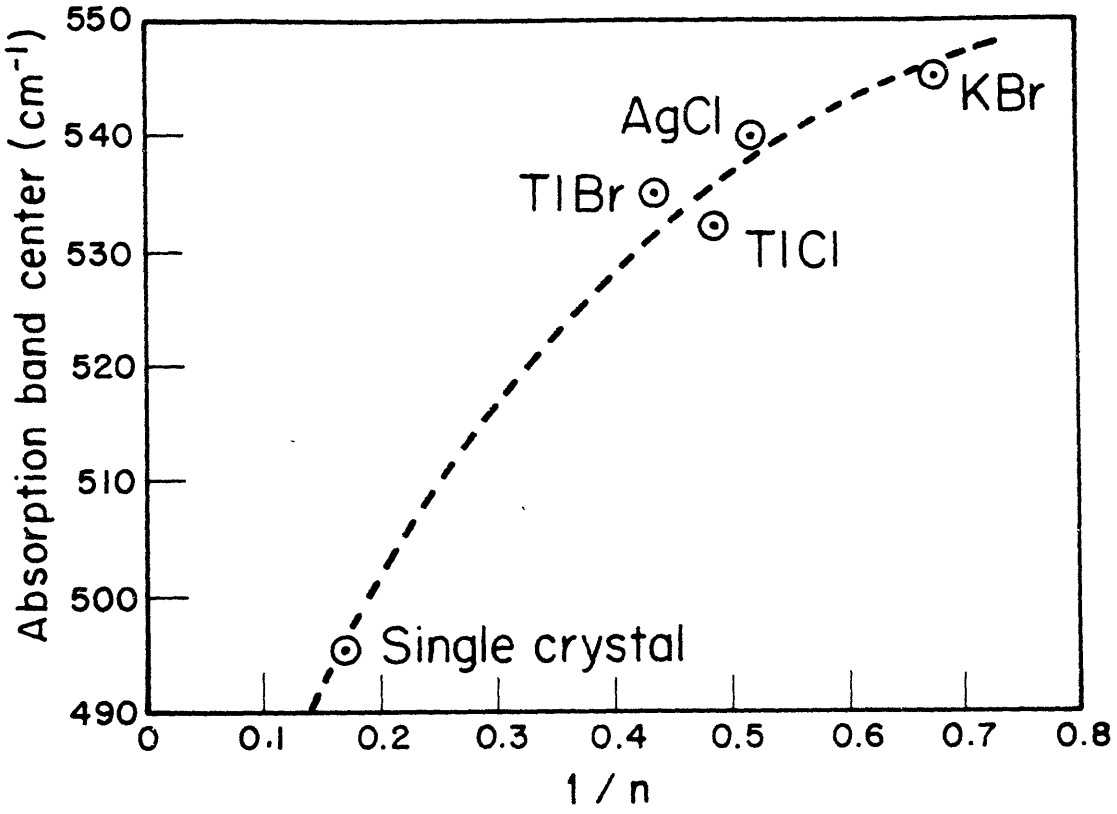

Fig. 26A. The absorption band center for powder $BaTiO_3$ as a function of the reciprocal index of refraction of the pressed disk matrix material.

measurements were made, these band centers lie at 590 cm^{-1} and 535 cm^{-1} (uncorrected for surface reflection), respectively. The shift is seen to be comparable for the two materials.

The problem of the shift in frequency when a powdered crystal is imbedded in a non-absorbing dielectric matrix, as well as the closely related problem of the change in absorption band intensity, is very difficult to treat quantitatively, because of the drastic simplifying assumptions

which must be made regarding the effect of particle interaction on the local field in the material. Theoretical investigations have been hindered also by the lack of accurate experimental information on band location and intensities.

The frequency shift of a dipole in a solvent liquid of dielectric constant k, considering electrostatic interactions between dipole and solvent, has been discussed by Kirkwood[27] and Bayliss[28], who showed that the dipole frequency shift should be proportional to $(1-k)/(2k+1)$, and to the intensity of the transition. This expression has been shown to be quantitatively correct only in a limited number of cases.[29]

The Kirkwood theory cannot explain the present data, although the observed trend towards lower frequency for single crystals and powder samples dispersed in higher dielectric constant matrices is in the predicted direction. Since the quantity of physical interest is the frequency of an oscillator when in the local field produced by the neighboring oscillators (i.e., a single crystal), a determination of the vibrational frequency of an isolated unit cell of the material is of minor importance.

The effect of the dielectric constant of a non-absorbing solvent on the intensity of the absorption band has been discussed by Chako[30] and Polo and Wilson[31] for the case of electronic absorption bands, using the classical theory of damped oscillators. For a solvent of index of refraction n, the intensity in the condensed phase was found to be greater than the gas phase intensity by a factor of $(n^2 + 2)^2/9n$. There is doubt on experimental grounds as to whether the intensity increase is as large as is given by this factor. In many cases, no intensity increase has

been observed.[32] For the case of a KBr matrix, with an index of refraction of about 1.5 at 500 cm^{-1}, the intensity increase on the Chako theory is about 30%.

The halfwidth of the high-frequency band in $BaTiO_3$ is about 100 cm^{-1} for single crystal samples and about 150 cm^{-1} for pressed disk samples. The $BaTiO_3$ in the pressed disk sample is less perfect due to the partial destruction of the crystal by the powdering operation, and increased interaction between optical and acoustic vibrations will thus be expected to increase the band width. This interaction will also prevent the absorption bands for the powder sample from sharpening at low temperatures as much as the single crystal bands, as observed experimentally (see Figs. 13, 15, and 19).

Since the diameter of the particles used is about a factor of 20 less than the incident wavelength, particle scattering will have a negligible effect on the band position and intensity. This was confirmed experimentally by using a powder about twice as coarse as the 1 micron size ordinarily used and observing no change in the absorption band.

Känzig[33] has postulated that there is a surface layer on $BaTiO_3$ extending to a depth of about 100A where the properties of the material are radically different from the bulk properties. For particles 1 micron (i.e., 2500 unit cell edges) in diameter, about 5% of the material lies in this surface layer. These surface effects, if present, would have little effect on the spectra.

Since it has not been possible to determine the absorption maximum in the single crystal spectrum corresponding to the pressed disk band at

about 400 cm^{-1}, the frequency of this band has been estimated from the shift between single crystal and pressed disk frequencies for the higher frequency band. The higher frequency band is located at about 545 cm^{-1} for a KBr pressed disk sample, and at 495 cm^{-1} for the single crystal sample corrected for surface reflectivity. The pressed disk frequency is lowered by about 15 cm^{-1} when the higher index powder TiCl is substituted for KBr.

For the low-frequency band, the KBr pressed disk frequency is 400 cm^{-1}, and is shifted about 40 cm^{-1} toward lower frequencies when a TlCl matrix is used. In view of the greater shift when a higher index powder is used, the frequency difference between the pressed disk and single crystal samples is probably greater for the low-frequency than for the high-frequency band. A value of 340 cm^{-1} has been chosen for the single crystal vibrational frequency, based on the powder shifts and on expected band halfwidths. This value is probably accurate to within 25 cm^{-1}.

3. Normal Vibrations of the Perovskite Lattice

An extensive body of theoretical and experimental evidence indicates that the absorption bands in the infrared spectra of solids are due to the excitation of optically active vibrations. In order to interpret these spectra, we can study the vibrations as wave motions in periodic structures. In this section, we shall qualitatively develop the complete vibrational spectrum of a cubic perovskite crystal, and indicate the requirements for modes which can be excited by infrared radiation. By the use of lattice symmetry arguments, the general form of the infrared

vibrations can be determined.

A crystal of $BaTiO_3$ containing N unit cells, each with 5 atoms, has 15N degrees of freedom. Of these 15N modes, there are 3N degrees of freedom related to translational motion and 3N degrees of freedom related to torsional motion of the unit cell. The remaining 9N modes are associated with vibrational degrees of freedom.

In the Born-von Kármán treatment of lattice vibrations[34], it is shown that each normal mode of a unit cell corresponds to N normal modes of the crystal, the wavelength associated with the lattice vibration determining the phase shift between adjacent unit cells. In the case of optically active vibrations, the phase of the lattice vibration must match that of the exciting electromagnetic wave. Since the unit cell dimensions are extremely small compared to the exciting infrared wavelength, the phase shift between neighboring cells is negligible, and all equivalent atoms in the lattice can be considered to vibrate in phase. A discussion of the vibrational frequencies of the unit cell will thus give information equivalent to a discussion of the vibrational frequencies of the complete lattice.

The 9 vibrations of the unit cell can be classified by a division into 3 vibrations of Ba against the TiO_3 group, and 6 internal TiO_3 vibrations. The interactions between these motions depend upon the masses and restoring forces of the vibrating atoms, and can be expected to be small in the case of $BaTiO_3$. The Ba-(TiO_3) vibrations can be treated by considering the TiO_3 group to be a single atom situated at the Ti position, and the vibrational problem that of a diatomic crystal of equivalent structure (e.g., the CsCl structure). In the cubic phase, this will lead to a

triply degenerate vibration since three equivalent axes exist.

To discuss the vibrational nature of the TiO_3 group, consider it to be arranged as a central Ti atom octahedrally surrounded by 6 oxygen half-atoms (Fig. 28a), to give the group the correct symmetry properties. This octahedron has the symmetry of the point group O_h, which has the 6 species of normal vibrations A_{1g}, E_g, F_{1u}, F_{1u}, F_{2u}, F_{2g}, as discussed by Herzberg.[35]

The requirement that atoms in equivalent positions in neighboring cells must perform the same vibrational motion reduces this set of normal vibrations to the two infrared-active vibrations of the species F_{1u}. The infrared-inactive vibrations of species F_{2u} are related to the torsional motion of the unit cell.

If we choose a vertical axis through a Ti-O chain, and label the two O half-atoms lying along this chain O_I and the four O half-atoms at right angles to this axis O_{II}, we can illustrate the two F_{1u} normal vibrations as shown in Fig. 27. In the first, a "stretching" vibration, the motion is primarily that of a change in length of the Ti-O_I bond (O_I and O_{II} up; Ti down); in the second, a "bending" vibration, the motion is primarily that of a change in the O_{II}-Ti-O_I bond angle (Ti and O_I up; O_{II} down). Both the relative magnitude and sign of the displacements will depend on the bond force constants and relative masses of the atoms. Since three equivalent axes exist in the case of the cubic lattice, both of these vibrations will be triply degenerate.

The degree of degeneracy of these two bands in structures of lower symmetry may be determined by resolving the symmetry types of the cubic point group into the point groups of lower symmetry. This re-arrangement

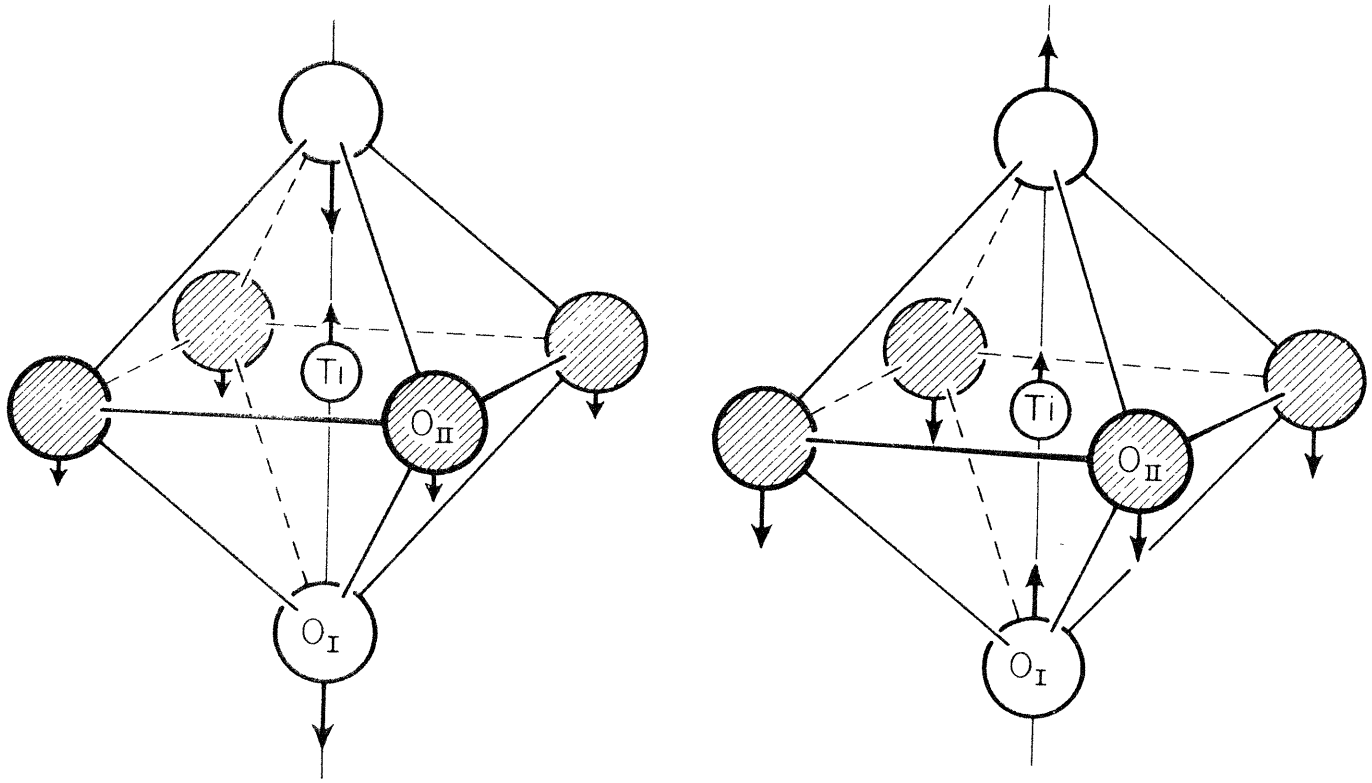

Fig. 27. Schematic infrared-active normal vibrations of a TiO_6 octahedron.
ν_1: higher frequency "stretching" vibration;
ν_2: lower frequency "bending" vibration.

Table V. Crystal symmetry and re-arrangement of symmetry species for the four phases of $BaTiO_3$.

Symmetry	Point group	Species	Expected band structure
Cubic	O_h	F_{1u}	Single band
Tetragonal	C_{4v}	E A_1	Double band
Orthorhombic	C_{2v}	B_1 B_2 A_1	Triple band
Rhombohedral	C_{3v}	E A_1	Double band

of symmetry types is shown in Table V. The cubic triple degeneracy is partially removed in the tetragonal structure and each of the bands is doubled. In the orthorhombic structure, the degeneracy is completely removed and each band is tripled. The symmetry species present in the rhombohedral structure are the same as those of the tetragonal structure and the bands are again doubled.

We thus expect three triply degenerate infrared-active vibration bands in the spectrum of cubic barium titanate, with the degeneracies partially or completely removed in the phases of lower symmetry.

4. Band Assignments

Infrared absorption bands have been observed in the vicinity of 500-600 cm^{-1} and 350-400 cm^{-1} for the vatious perovskite titanates investigated (Table IV). The higher frequency band, ν_1, will be assigned to the

$Ti\text{-}O_I$ "stretching" normal vibration (Fig. 27a), the lower, ν_2, to the $Ti\text{-}O_{II}$ "bending" normal vibration (Fig. 27b), and a low-frequency band, ν_3, at frequencies lower than the available experimental range, to the cation-(TiO_3) vibration, for the reasons discussed below.

The two observed vibrations ν_1 and ν_2 are of approximately equal intensity, as expected if motions of the same types of ions are involved. The two bands occur in the spectral region where bands due predominatly to vibrations between oxygen and metal cations are commonly observed, as in MgO (580 cm^{-1})[36], TiO_2 (ca. 550 cm^{-1} and 250 cm^{-1})[4], and Fe_3O_4 (570 cm^{-1} and 380 cm^{-1}).[3]

The stretching vibration is expected to occur at higher frequency than the bending vibration on the basis of empirical evidence on a large number of molecules, and on the following electrostatic considerations. The principal changes in interatomic distances for the stretching and bending vibrations involve the $Ti\text{-}O_I$ and O_{II}-Ba interatomic distances, respectively. If we make the simplifying assumptions that the interatomic forces in the $BaTiO_3$ lattice are determined as if the Coulomb attraction and closed shell repulsion forces are balanced separately for each bond, and that the structure is ionic, the Coulomb attraction force will be four times as great along the Ti-O bond as along the Ba-O bond, since the Ti charge is twice as great as the Ba charge, and the Ti-O distance is $\sqrt{2}$ less. Using the force balance assumption, the ratio of the closed shell repulsion forces will therefore also be a factor of four. This closed shell repulsion force may be described roughly as being of the form r^{-n}, where n is of the order of 8. The force constant, the derivative of the force with respect to distance, will receive its major contribution

from this repulsion term rather than from Coulomb attraction terms at the equilibrium position. The force constant ratio for the two bonds will therefore be approximately four, the same as the repulsion force ratio, and the frequency ratio will therefore be about two. This frequency difference will be decreased somewhat when the covalent nature of the bonds and the effect of O-O repulsion are taken into account.

The frequency of the unobserved vibration ν_3 can be estimated roughly by considering this vibration to take place between a Ba atom and an atom with the charge and mass of the TiO_3 group, and comparing this vibration with that of a divalent diatomic ionic lattice having the same reduced mass, whose vibrational frequency has been measured by residual ray or thin crystal absorption measurements. Unfortunately, no divalent lattices having a reduced mass near 57, that of Ba-(TiO_3), have been measured. A comparison can be made with the monovalent ionic lattices CsBr and RbI[37], having reduced masses of 50 and 51, and frequencies of 75 cm^{-1} and 77 cm^{-1}, if a correction is made for the fact that the ionic charge is only half as great as in the Ba-(TiO_3) lattice. Using simple electrostatic arguments, the effect of doubling the charge on each atom is to increase the force constant by a factor of four, and thus to double the vibrational frequency. Slight additional increases will probably be caused by additional repulsion terms. Considering these corrections, the frequency of the Ba-(TiO_3) vibration ν_3 can be expected to occur at about 150-200 cm^{-1}.

5. Force Constants

The vibrational frequencies for normal vibrations of a system of

coupled harmonic oscillators can be computed from the masses of the particles and the restoring forces between particles, using the equations of motion. The problem which usually arises in the course of infrared investigations is that of using measured vibrational frequencies and known atomic masses to determine the interatomic forces.

In principle, an exact form of the potential energy curve for a system of N harmonically bound particles, in terms of the force constants k_{ij} and the displacements from equilibrium q_i may be represented by a series of the form

$$V = 1/2 \sum_{i,j=1}^{3N} k_{ij} q_i q_j \quad .$$

The equations of motion of the system can be represented by

$$m_i \ddot{q}_i + \sum_{j=1}^{3N} k_{ij} q_j = 0 \qquad i = 1,2, \ldots 3N$$

with a solution, for harmonic motion of frequency ω,

$$q_i = A_i \cos (\omega t - \delta) \quad .$$

Thus,

$$\sum_j (k_{ij} - m_i \omega^2 \delta_{ij}) \, q_i = 0 \quad .$$

This has a non-zero solution only when the secular equation vanishes:

$$\left| k_{ij} - \delta_{ij} m_i \omega^2 \right| = 0 \quad .$$

The number of force constants which can be determined by this method is thus equal to the number of known vibrational frequencies.

In the present case, the potential energy is assumed to have the form

$$V = 1/2 \sum k_s q_s^2 + 1/2 \sum k_b q_b^2 \quad ,$$

where $q_s = \Delta z_{Ti} - \Delta z_{O_I}$ and $q_b = \Delta z_{Ti} - \Delta z_{O_{II}}$, where z is the atomic co-ordinate in the Ti-O_I direction, and k_s and k_b are the corresponding force constants. The use of this potential function amounts to treating the vibrations of the TiO_3 group separately from the Ba-(TiO_3) vibrations. This approximation is justified in the present case since little interaction occurs between the two sets of vibrations.

Since there are only two independent force constants k_s and k_b for the TiO_3 group in the cubic perovskite structure, the octahedron as shown in Fig. 28a may be replaced by a simpler structure, equivalent from the standpoint of the force constant calculation.

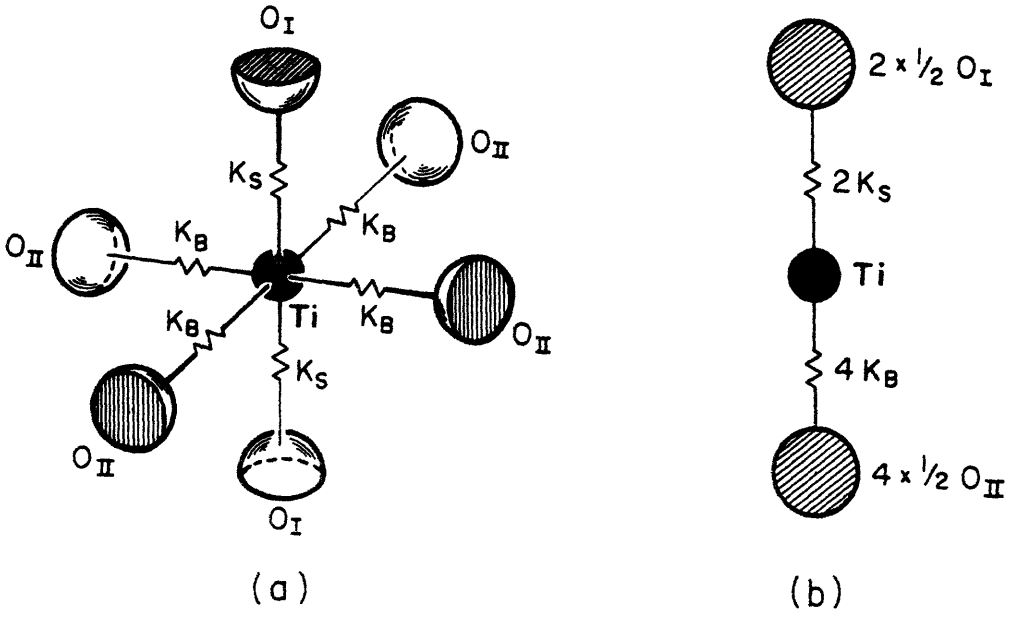

Fig. 28. (a) The TiO_3 group in cubic $BaTiO_3$.
(b) An equivalent arrangement for force constant calculations.

The two O_I half-atoms perform identical motions during the normal vibration. The momentum of the system and the vibrational frequency are unchanged if the lower O_I half-atom is translated until it occupies the position of the upper one, and the force constant k_s is doubled.

Likewise, since the four O_{II} half-atoms carry out identical motions, three of them can be rotated until they occupy the position of the fourth. The force constant must now be multiplied by four. This system is not completely equivalent to the original one, since now there is a net angular momentum when the system vibrates, due to the fact that the counterbalancing effect of the O_{II} half-atoms on opposite sides of the Ti-O_I axis has been destroyed. The motion of the O_{II} atoms is in the same direction as the motion of the other atoms. Therefore, the O_{II} atoms can be displaced until they lie on the Ti-O_I axis at the point formerly occupied by the lower O_I half-atom. This linear system (Fig. 28b) will have no net linear or angular momentum during the normal vibrations, and will have the same vibrational frequencies as the original octahedron.

The force constants k_s and k_b for the normal vibrations may be obtained by solving the secular equation:

$$\begin{vmatrix} (\mu_o + \mu_1)\ (2k_s) - \lambda & -\mu_o(4k_b) \\ -\mu_o(2k_s) & (\mu_o + \mu_2)\ (4k_b) - \lambda \end{vmatrix} = 0 \quad ,$$

where μ_o = reciprocal mass of Ti, μ_1 = reciprocal mass of O_I, μ_2 = reciprocal mass of $2O_{II}$, $\lambda = (2\pi\nu)^2$. If we call $A = \mu_o + \mu_1$, $B = \mu_o + \mu_2$, $D = \mu_o\mu_1 + \mu_o\mu_2 + \mu_1\mu_2$, $\frac{\sqrt{\lambda_1}}{2\pi}$ and $\frac{\sqrt{\lambda_2}}{2\pi}$ the two observed frequencies, we obtain

$$2k_s = \frac{\lambda_1 + \lambda_2}{2A}\left[1 + \sqrt{1 - \frac{4BA}{D}\frac{\lambda_1\lambda_2}{(\lambda_1 + \lambda_2)^2}}\right]$$

$$4k_b = \frac{\lambda_1 + \lambda_2}{2B}\left[1 - \sqrt{1 - \frac{4BA}{D}\frac{\lambda_1\lambda_2}{(\lambda_1 + \lambda_2)^2}}\right].$$

Force constants for $BaTiO_3$, $SrTiO_3$, $PbTiO_3$, $KNbO_3$, and $NaNbO_3$, using the powder sample frequencies of Table III, and for single crystal $BaTiO_3$, using frequencies of 495 cm^{-1} and 340 cm^{-1}, are shown in Table VI. In these calculations, the slight departure from a cubic structure which occurs in all materials except $SrTiO_3$ has been neglected.

Table VI. Computed force constants.

	k_s dynes/cm	k_b dynes/cm
$BaTiO_3$ (single crystal)	0.753×10^5	0.417×10^5
$BaTiO_3$ (powder)	0.798	0.638*
$SrTiO_3$ (powder)	1.16	0.561
$PbTiO_3$ (powder)	1.04	0.602
$KNbO_3$ (powder)	1.72	0.521
$NaNbO_3$ (powder)	1.80	0.521

* The force constants for the $BaTiO_3$ powder sample are slightly imaginary for the observed frequencies. Neglecting this very small imaginary part leads to the listed force constants and to frequencies separated by about 5 cm^{-1} more than the observed frequencies.

For the force constants for $BaTiO_3$ computed using the two sets of data, the stretching force constant is about 5% lower for the single-crystal data than for the powder data, and the bending force constant is about 30% lower. The force constants computed for the other materials, for which only powder data are available, are probably also somewhat higher than those corresponding to single crystal frequencies.

6. Specific Heat Contributions

Two infrared-active vibrations of the $BaTiO_3$ lattice have been measured, and a third lower frequency vibration, a vibration of Ba against the TiO_3 group, has been predicted on the basis of the number of degrees of freedom of the system and the crystal symmetry. This low frequency vibration has been estimated to lie in the range of 150 - 200 cm^{-1} by comparing the Ba-(TiO_3) lattice with ionic crystals for which the fundamental lattice vibrations have been measured. A comparison of the measured low temperature specific heat curve with that computed from the sum of the Einstein and Debye specific heat contributions of the various optical and acoustic vibrations may be used to determine this third frequency more accurately.

As discussed earlier, the 15 degrees of freedom of the $BaTiO_3$ unit cell can be separated into three degrees associated with lattice translations, three with infrared-inactive torsional vibrations of species F_{2u}, and three with each of the three infrared-active vibrations. The translational modes will introduce a Debye contribution to the specific heat; the others will be treated as Einstein contributions.

The two measured vibrations $\nu_1 = 495\ cm^{-1}$ and $\nu_2 = 340\ cm^{-1}$ have Einstein temperatures of 720°C and 490°C. The torsional vibration has a motion similar to that of the infrared-active "bending" vibration ν_2; the Einstein temperatures of these two vibrations will be assumed to be the same. The ratio of the frequency of the Ba-(TiO_3) vibration ν_3 to the limiting translational frequency can be estimated by considering the TiO_3 group to be a single atom, and the Ba-(TiO_3) crystal as a diatomic lattice having the CsCl structure. The infrared-active frequency of this lattice, the same as that of a one dimensional diatomic chain, is [38]

$$\nu_{opt} = \frac{1}{2\pi}\sqrt{\frac{M+m}{Mm}(2k)} \quad ,$$

and the maximum translational frequency

$$\nu_{acoust} = \frac{1}{2\pi}\sqrt{\frac{2k}{M}} \quad ,$$

where $M > m$, and k is the force constant associated with the vibration. In the present case, the ratio of the two frequencies is

$$\frac{\nu_{acoust}}{\nu_{opt}} = \sqrt{\frac{m_{TiO_3}}{m_{TiO_3} + M_{Ba}}} = 0.64 \quad .$$

The molar specific heat under these assumptions is

$$C_v = 3R\left[f_E\left(\frac{T}{720}\right) + 2f_E\left(\frac{I}{490}\right) + f_E\left(\frac{T}{T_3}\right) + f_D\left(\frac{T}{0.64\ T_3}\right)\right] .$$

The Einstein temperature T_3 for the vibration ν_3 which will lead to an agreement with experimental values of the specific heat[39] can thus be determined.

The measured C_p values may be converted to C_v values by using the thermal expansion coefficients given by Megaw[11] and Rhodes[40], and values

Table VII. Specific heat contributions of the $BaTiO_3$ lattice vibrations.

Temp. (°K)	C_p [39]	C_v*	$f_E\left(\frac{T}{720}\right)$	$2f_E\left(\frac{T}{490}\right)$	$f_E\left(\frac{T}{T_3}\right)+f_D\left(\frac{T}{0.64\ T_3}\right)$	T_3 (°K)	3 (cm^{-1})
55	4.19	4.12	0.002	0.13	4.0	312	220
75	7.0	6.9	0.04	0.76	6.1	304	210
100	10.3	10.2	0.23	2.20	7.8	312	220
125	13.3	13.1	0.63	3.80	8.7	328	230
150	16.0	15.8	1.15	5.30	9.4	335	235
175	18.2	18.0	1.70	6.48	9.8	351	245

* A correction $C_p - C_v = 0.0014\ T$ has been assumed.

for the compressibility computed from the elastic constant data of Bond, Mason, and McSkimin.[41] This small $C_p - C_v$ correction, assumed to be linear with temperature, is 0.0014T.

The values of the Einstein temperature for the vibration ν_3 computed on this basis are shown in Table VII. The Einstein temperature best fitting the low-temperature data is about 320°K, corresponding to a vibrational frequency of 225 cm^{-1}. Using the one dimensional diatomic lattice approximation, this leads to a force constant $k_3 = 0.84 \times 10^5$ dynes/cm for the Ba-(TiO_3) vibration. When referred to the CsCl arrangement, k_3 is related to the change in separation of a plane of Ba atoms on the unit cell face and the TiO_3 group at the center of the unit cell,

directed along a [100] or equivalent direction. The force constant $k_t = 0.63 \times 10^5$ dynes/cm for a Ba-(TiO_3) bond directed along a cube body diagonal is 3/4 as large as k_3, since there are eight bonds involved instead of six.

7. Compressibility and Elastic Constants

Considering $BaTiO_3$ as cubic, the compressibility can be computed from the stretching force constants, k_s for the Ti-O bond and k_t for the Ba-(TiO_3) bond. For unit contraction along the three axes of the unit cell, 6 Ti-O bonds are each shortened a distance 1/2, and 8 Ba-(TiO_3) bonds are each shortened a distance $\sqrt{3}/2$. The energy for unit compression is thus:

$$U = \frac{3}{4} k_s + 3 k_t \quad .$$

The energy density of a compressed crystal may be expressed in terms of the elastic constants c_{ij} and the strain and shear components α_i by:[42]

$$\tilde{U} = \frac{1}{2} \sum_{i,j=1}^{6} c_{ij} \alpha_i \alpha_j \quad .$$

For unit compression of a cubic unit cell of edge length L, this becomes

$$U = \tilde{U} L^3 = \frac{3}{2} L \, (c_{11} + 2c_{12})$$

since $\alpha_i^2 = 1/L^2$. The elastic constants may be replaced by the cubic compressibility through

$$\beta = \frac{3}{c_{11} + 2c_{12}} \quad .$$

The compressibility in terms of the force constants for $BaTiO_3$ is thus

$$\beta = \frac{6L}{k_s + 4k_t} \quad .$$

Using values $k_s = 0.75 \times 10^5$ dynes/cm, $k_t = 0.63 \times 10^5$ dynes/cm, and $L = 4.0 \times 10^{-8}$ cm, the compressibility $\beta = 7.3 \times 10^{-13}$ cm^2/dyne. This can be compared with a value for the compressibility of 6.17×10^{-13} cm^2/dyne, computed from the elastic constant data determined for single-crystal $BaTiO_3$ by Bond, Mason, and McSkimin.[41] ($c_{11} = 2.06 \times 10^{12}$ dynes/cm^2; $c_{12} = 1.40 \times 10^{12}$ dynes/cm^2.) The agreement is reasonable, considering the potential approximations used, and the assumption of cubic symmetry.

A value for the elastic constant c_{11} may be determined directly from the stretching force constants. For a unit linear contraction of one unit cell, two Ti-O bonds are shortened a distance 1/2, and 8 Ba-(TiO_3) bonds are shortened $1/2\sqrt{3}$, which leads to the energy relationships

$$U = \frac{k_s}{4} + \frac{k_t}{3} = \frac{1}{2} c_{11} L \quad .$$

The elastic constant c_{11} is thus

$$c_{11} = \frac{1}{L} \left(\frac{k_s}{2} + \frac{2k_t}{3} \right) = 2.00 \times 10^{-13} \text{ dynes/cm}^2,$$

in excellent agreement with the value $c_{11} = 2.06 \times 10^{-13}$ dynes/cm^2, determined experimentally by Bond, Mason, and McSkimin.

8. Band Intensities

Information concerning the change in electric dipole moment with interatomic distance can be obtained from the integrated intensity of infrared absorption bands. The change in dipole moment obtained for a normal vibration is the vector sum of the changes in dipole moments of the individual bonds. To determine this vector sum, the band intensities were measured for ν_1 and ν_2 for the powder spectra of $BaTiO_3$, $PbTiO_3$, $SrTiO_3$, $KNbO_3$, and $NaNbO_3$.

The extinction coefficient k is defined by

$$\frac{I_{trans}}{I_{inc}} = e^{-kx} \quad ,$$

where I is the intensity of the radiation and x is the path length. It can be shown, for the case of a system of gas molecules, that the integrated absorption band intensity[43]

$$\bar{k} = \int k(\nu)\, d\nu = \frac{8\pi^3 N}{3ch} \left[[M]^{n,m} \right]^2 \quad ,$$

where N is the number of molecules per unit volume, ν is the frequency, c is the velocity of light, h is Planck's constant, and

$$[M]^{n,m} = \int \psi_n \mu \psi_m^* \, d\tau$$

is the matrix element corresponding to the electric dipole transition between the states m and n. This transition moment may be expanded in a power series in the normal co-ordinate q

$$[M]^{n,m} = M_o \int \psi_n \psi_m^* d\tau + \frac{dM}{dq} \int \psi_n q \psi_m^* d\tau + \frac{1}{2} \frac{d^2M}{dq^2} \int \psi_n q^2 \psi_m^* d\tau + \ldots$$

The first term vanishes since the wave functions are orthogonal. The third term is zero in the harmonic oscillator approximation for fundamental absorption bands. For harmonic oscillators, the integral giving the transition probability between the ground state and the first excited state is

$$q^{0.1} = \int \psi_n q \, \psi_m^* d = \frac{1}{\sqrt{2\alpha}} \quad ,$$

where $\alpha = 4\pi^2 mc\nu / h$ where m is the reduced mass. The change of electric dipole moment with normal co-ordinate distance is thus:

$$\left(\frac{dM}{dq}\right)^2 = \frac{3\alpha ch}{4\pi^3 N} \bar{k} = \frac{3mc^2}{\pi N x} \bar{k}x \quad .$$

(The path length x has been included as a computational aid.)

Band areas from the powder data of Figs. 21 and 25 have been used. Since the low-frequency edge of band ν_2 could not be measured in most cases, the area under this band was determined from the curve half-width areas and the band shape. The normal vibrations are not pure bending or stretching vibrations; the reduced mass used was that satisfying the energy and momentum relationships for the normal motions computed from the force constants. Table VIII shows the values of $\left|\frac{dM}{dq}\right|$ for $BaTiO_3$, $SrTiO_3$, $PbTiO_3$, $KNbO_3$, and $NaNbO_3$, for the vibrations ν_1 and ν_2. In addition, the effective charge of the vibrating system was determined by the relationship

$$Q = \left|\frac{dM}{dq}\right| / \sqrt{3}\,\epsilon \quad ,$$

where ϵ is the electronic charge. Since the vibrations are triply degenerate, the factor of $\sqrt{3}$ must be included to yield the correct value for a single axis.

It is possible in theory to extend these calculations to separate the vector sum of $\left|\frac{dM}{dq}\right|$ computed above to determine the individual change in dipole moment for each bond taking place in the normal vibration. This extension will not be made, since the results of such a calculation are strongly dependent on the exact form of the normal vibrations, known only approximately due to the simplifying assumptions made in calculating the force constants. Values for the individual bond contributions would be useful only if known fairly accurately.

The values obtained for $\left|\frac{dM}{dq}\right|$ are similar for all of the perovskite materials investigated, and are close to the values found by Waldron[3] for various ferrites, where the normal vibrations are also primarily

Table VIII. Band intensities and derived constants.

Compound	Fundamental	$\bar{k}x$ (cm^{-1})	Nx (cm^{-2}) x10^{18}	m (atomic mass units)	$\left\|\frac{dM}{dq}\right\|$ (esu) x10^{-9}	Q(ε)
$BaTiO_3$	ν_1	269	1.48	5.8	1.23	1.44
	ν_2	203	1.48	10.6	1.44	1.73
$PbTiO_3$	ν_1	362	1.74	5.8	1.32	1.57
	ν_2	118	1.74	12.3	1.10	1.32
$SrTiO_3$	ν_1	253	0.99	5.9	1.47	1.76
	ν_2	125	0.99	13.4	1.56	1.87
$KNbO_3$	ν_1	253	1.06	9.2	1.77	2.12
	ν_2	57	1.06	20.2	1.25	1.50
$NaNbO_3$	ν_1	262	1.10	9.3	1.78	2.14
	ν_2	39	1.10	20.2	1.02	1.22

those of oxygen ions. Since the value for the change in dipole moment obtained for $BaTiO_3$ is no larger than that obtained for these other non-ferroelectric materials, there is no abnormally large effective charge in $BaTiO_3$ for the vibrations in the region investigated.

9. Single Crystal Spectra

A discussion of the infrared spectrum of $BaTiO_3$ to this point has dealt with the expected normal vibrations of the unit cell, and the use

of these vibrational frequencies to determine the interatomic force constants, the vibrational specific heat contributions, and band intensities. In these discussions and computations, the slight departure of the lattice from the cubic perovskite structure has been ignored. The effect on the spectrum of the symmetry changes occurring at the various phase transitions will now be discussed.

The infrared spectrum of $BaTiO_3$ has been observed in the four phases for on single crystal samples only on the higher frequency band ν_1, due to the low signal to noise ratio at lower frequencies, and problems due to high crystal reflectivity at low frequencies. The same band splitting was observed for pressed disk samples in the various phases, but since the phase transitions are sluggish in the powder samples, a discussion of the differences among the spectra of the four phases will be confined to the single crystal measurements.

The comparison of primary interest is that of the cubic and tetragonal spectra, since the material becomes ferroelectric when it undergoes the transition to the tetragonal state. The slightly broader band in the tetragonal spectrum (Fig. 14) is expected since this band is now doubly rather than triply degenerate. The band intensities are equal for the two phases. This indicates that the frequency difference between vibrations along and at right angles to the polar axis is slight; if one of the components of the tetragonal band underwent a large frequency change at the transition, it would shift out of the range of observation and the tetragonal band intensity would decrease markedly. Measurements of the maximum absorption while the temperature was slowly

lowered through the Curie point indicated no anomalous intensity jump that could not be explained by the slight shift of band center; this indicates that there is no radical change in the dipole moment with interatomic separation at the transition point.

The polarized light measurements on the tetragonal crystal (Fig. 14) show that the vibrational frequency along the polar axis is about 20 cm^{-1} higher than that at right angles to the polar axis. Since the unit cell is about 1% longer along the polar axis, this seems to violate the general rule that the vibrational frequency is decreased when the bond distance is increased. As has been shown by X-ray and neutron diffraction measurements (Table II), the Ti ion is displaced in the tetragonal phase to a non-central position in the oxygen octahedron, so that there are two $Ti\text{-}O_I$ distances along the polar axis of 1.87A and 2.14A, as compared to the $Ti\text{-}O_{II}$ distance of 1.997A at right angles to the polar axis.

As discussed earlier, the force constant depends strongly on the short-order closed shell repulsion forces. The force constant will therefore be more sensitive to a decrease of bond length than to an increase. Therefore, although there is a net increase in the average bond distance, the greater effect of decreasing one bond increases the overall force constant and thus the vibrational frequency. The Ti-O distance at right angles to the polar axis is practically the same as the Ti-O distance of 2.004A in the cubic phase. The fact that the same vibrational frequency of 495 cm^{-1} has been observed for each of these vibrations indicates that no large rearrangement of charges takes place at right angles to the polar axis when $BaTiO_3$ becomes tetragonal.

The symmetry arguments advanced earlier predicted that the degeneracy should be completely removed in the orthorhombic phase and that the band should be tripled. However, two of the unit cell dimensions are practically the same, and the slight frequency difference between these vibrations cannot be resolved. The shoulder on this band (Fig. 16) becomes stronger as the temperature is lowered but as far as can be determined there is no frequency shift. The increase in strength is due to normal low temperature sharpening effects and also perhaps to domain rearrangement. Since the domain patterns are complicated in the orthorhombic phase it was not possible to perform the polarized light measurements carried out at room temperature.

The rhombohedral band has the same double degeneracy as the tetragonal band, and a double band is observed. As the temperature is lowered, the lower frequency component becomes more intense while the higher component remains practically constant in intensity; again, this can be ascribed to a combination of low temperature sharpening and domain rearrangement effects. Since the band frequencies do not change with temperature in this phase, there are probably no atomic shifts below the transition point.

The explanation of the observed low-temperature spectra on the basis of the change in symmetry properties is strengthened by the distinct changes in the spectra near temperatures where phase transitions are known to occur, and by the absence of changes in band shape and intensity in the low-temperature spectrum of hexagonal barium titanate, prepared from the same starting materials as the perovskite form.

The infrared spectrum of barium titanate in the region investigated

can thus be explained on the grounds of crystal symmetry and known atomic positions if intensity complications caused by different possible domain orientations are taken into account; nothing has been observed which can be related directly to ferroelectric effects.

10. Effect of Cation Replacement

Since the spectra of thin single crystals have been measured only for $BaTiO_3$ and $PbTiO_3$, and reflection measurements are so broad that little information can be obtained from them, a comparison of the spectra to determine the effect of cation substitution will deal primarily with the pressed disk measurements, where the spectra could be measured under the same conditions for each material. The cation substitution may be expected to cause spectral changes due to alterations in unit cell size, crystal structure, and binding energy.

The qualitative similarity of the powder spectra of $BaTiO_3$, $SrTiO_3$, and $PbTiO_3$ is expected in view of the assignment of the observed absorption bands to normal vibrations of the TiO_6 octahedron. In Table IX, the frequency and halfwidth of the vibration bands ν_1 and ν_2 are listed, together with the unit cell dimensions, and the Ti-O distance along the polar axis as determined by X-ray and neutron diffraction measurements.

The observed band locations can be explained by an inverse relationship between atomic separation and vibrational frequency; the band halfwidths by the degree of degeneracy of the band, and the resulting departure from cubic symmetry. $SrTiO_3$ is cubic, and band ν_1 is narrower than this band in the tetragonal materials $BaTiO_3$ and $PbTiO_3$. The band

Table IX

Vibration bands, band halfwidths, and unit cell dimensions for $SrTiO_3$, $BaTiO_3$ and $PbTiO_3$.

Material	ν_1	Halfwidth ν_1	ν_2	Halfwidth ν_2	"c" axis	"a" axis	Ti-O distance
$SrTiO_3$	610 cm^{-1}	145 cm^{-1}	395 cm^{-1}	130 cm^{-1}	3.897A	3.897A	1.948A
$BaTiO_3$	545 cm^{-1}	160 cm^{-1}	400 cm^{-1}	125 cm^{-1}	4.034A	3.994A	1.86*
$PbTiO_3$	590 cm^{-1}	215 cm^{-1}	405 cm^{-1}	150 cm^{-1}	4.152A	3.90A	1.79*

* The shorter Ti-O distance along the polar axis ("c" axis) is listed.

halfwidth in $BaTiO_3$ is about 15 cm^{-1} greater than that of $SrTiO_3$, and that of $PbTiO_3$ is about 60 cm^{-1} greater, about the separations observed between the two components of this band from the single crystal measurements (Figs. 20 and 21). As discussed earlier, the higher frequency component of band ν_1 in $BaTiO_3$ is due to the Ti-O vibration along the polar axis, even though the unit cell is longer in this direction. The same is probably true for $PbTiO_3$, since the displacement of the Ti atom from its central position in the TiO_6 octahedron, which causes the frequency increase in $BaTiO_3$, is even more pronounced in the case of $PbTiO_3$. It was not possible to confirm this frequency assignment experimentally since the polarized light measurements carried out on $BaTiO_3$ could not be performed on $PbTiO_3$ due to the difficulty of obtaining single-domain crystals.

The lower frequency band ν_2 occurs at the same frequency in the three materials. This bending vibration can be described as a change in the O_{II}-cation distance. If the lattice size is determined by this distance, rather than by the Ti-O distance, the interatomic forces and thus the vibrational frequency would be expected to be the same for the three materials. It has been impossible to determine fine structure in this band ν_2 for the non-cubic materials; however, it can be seen that ν_2 in $BaTiO_3$ and $PbTiO_3$ is less symmetric than in $SrTiO_3$.

$CaTiO_3$, which has an orthorhombic perovskite structure, exhibits the same double band spectrum (Fig. 23) observed for orthorhombic $BaTiO_3$, but with additional fine structure. Since it is not known if the observed fine structure is due to lowered symmetry caused by the puckered nature of the octahedron in this material[44] or to unreacted components

present, no interpretation will be placed on this spectrum.

In the ilmenite structure exhibited by $MgTiO_3$ and $ZnTiO_3$, the the oxygen atoms are arranged in a warped hexagonal close packing, with one-third of the interstices filled with Mg atoms, one-third with Ti, and one-third vacant.[45] Each Ti atom is surrounded by six O atoms, as in the perovskite modification, but the Ti-O chains present in the perovskite form no longer occur. In the observed spectra (Figs. 23 and 24), the band corresponding to the perovskite Ti-O stretching vibration is seen to be located in about the same position, although exhibiting much fine structure. The band corresponding to the lower frequency vibration ν_2 becomes doubled, due to the symmetry changes and the radically changed O-O repulsion forces.

$CdTiO_3$ can have either the perovskite or ilmenite structure, depending on the firing temperature.[45] The material used in this investigation has the ilmenite form, judging by the observed double low-frequency band.

The spectra of the orthorhombic perovskite $KNbO_3$ and $NaNbO_3$ (Fig. 25) are similar to that of orthorhombic $BaTiO_3$, with a shoulder on the low-frequency side of the high-frequency band ν_1, which adds weight to the assignment of the observed fine structure to symmetry effects. The vibrations ν_1 and ν_2 are primarily motions of oxygen atoms, so it is reasonable that there is little difference between the titanate and niobate spectra. The niobate frequencies ν_1 are slightly higher than that for $BaTiO_3$, due to the smaller lattice size (Table X) and the fact that the Nb atom has a higher charge than Ti, increasing the Nb-O force constant. Band ν_2 occurs at lower frequency in the

Table X. Orthorhombic perovskite unit cell dimensions (after Vousden[12]).

	a	c	b
$BaTiO_3$ (-10°C)	5.682A	5.669A	3.990A
$KNbO_3$ (room temp.)	5.720	5.694	3.971
$NaNbO_3$ (room temp.)	5.568	5.505	3.880

niobates than the titanates. The forces between oxygen and the monovalent cation K or Nb are less than the forces between oxygen and the divalent cations in the niobates. The low-frequency shoulder on band ν_1 is located about 100 cm^{-1} below the band center in $KNbO_3$ and about 150 cm^{-1} in $NaNbO_3$, compared to about 15 cm^{-1} in orthorhombic $BaTiO_3$. The orthorhombic $BaTiO_3$ structure is more nearly tetragonal than the orthorhombic niobates. The angles between the diagonals of the base of the orthorhombic unit cells are 90°8' in $BaTiO_3$, 90°16' in $KNbO_3$, and 90°40' in $NaNbO_3$.[12]

$KNbO_3$ is ferroelectric at room temperature, while $NaNbO_3$ is antiferroelectric. In the ferroelectric arrangement, the slight atomic displacements from a symmetrical arrangement are in the same direction in all unit cells; in the antiferroelectric arrangement, neighboring cells have displacements in opposite directions. No differences between the spectra of $KNbO_3$ and $NaNbO_3$ were present which could be related to this effect.

It is not possible to usefully compare the various band intensities, due to the fact that the observed intensities are proportional to the vector sums of the change of dipole moment with a change in normal coordinate, and not to the individual moment changes.

11. Dielectric Constants

A quantitative relationship between the infrared absorption band intensity and frequency and the contribution of this atomic vibration to the static dielectric constant requires detailed information regarding the effect of the local field on the total intensity of the absorption band, and thus knowledge of the effect of particle interaction on the oscillator transition probability. For the case of ionic crystals such as NaCl, where the local field can be determined fairly accurately by simplified theories, the contribution of the ionic vibrations to the static dielectric constant can be determined to within about 20%.[46] For crystals having partial covalent binding, where the dipole moment may change rapidly with internuclear separation, the agreement is much less satisfactory, and such calculations are of little value.

The perovskite titanates, as well as TiO_2 and hexagonal $BaTiO_3$, have a TiO_6 octahedron as the basic structural element, and are characterized by high dielectric constants (Table XI). Aside from the extremely high "a" dielectric constant (at right angles to the polar axis) in ferroelectric $BaTiO_3$, these dielectric constants have approximately the same value, and can be attributed to the Ti-O polarizability. Thus, for TiO_2, it has been possible to compute the optical constants in the infrared by fitting the reflection curves of Liebisch and Rubens (Fig. 1)

Table XI. Static dielectric constants.

	Field direction	Dielectric constant	Reference
$BaTiO_3$	"c" axis	155	(47)
$BaTiO_3$	"a" axis	5000	(10)
Hex. $BaTiO_3$	"c" axis	245	(50)
Hex. $BaTiO_3$	"a" axis	65	(50)
TiO_2	"c" axis	200	(49)
TiO_2	"a" axis	87	(49)
$SrTiO_3$	(ceramic)	234	(49)
$CaTiO_3$	(ceramic)	167.8	(49)
$PbTiO_3$	(ceramic)	100	(51)

by a two region dispersion formula.[5] Below the lowest frequency absorption band, centered at about 250 cm^{-1}, the refractive indices attain values which lead to dielectric constants in good agreement with the static values.

For $BaTiO_3$, with the lowest frequency band predicted at ca. 225 cm^{-1}, the "c" dielectric constant is expected to have a practically constant value from electrical frequencies to the onset of this low frequency vibration. (The $BaTiO_3$ "c" dielectric constant referred to here is that for a crystal with zero average polarization, where there are no electromechanical contributions to the dielectric constant, as discussed by Drougard and Young.[47])

It has been observed experimentally that the vibrational frequency for the high-frequency vibration ν_1 in $BaTiO_3$ has practically the same value along the "a" and "c" axes. No intensity shift was observed at the Curie point for the vibrations ν_1 and ν_2, indicating that there is no band component shifting to low frequencies when the material becomes ferroelectric. This evidence indicates that the potential well at infrared frequencies is almost the same in the two directions, and therefore there will be little difference in the dielectric constants at these frequencies.

As discussed by Forsbergh[48], the free energy for the tetragonal and orthorhombic phases is practically the same at room temperature. It therefore requires little energy to move the atoms in the tetragonal phase to an arrangement closer to that of the orthorhombic phase if the crystal is free to simultaneously distort and shear slightly. This leads to a very high dielectric constant in the "a" direction. At high frequencies, this required distortion can no longer take place in the crystal, and the potential wells will be similar in the "a" and "c" directions, as observed by the infrared measurements.

The dielectric constants for the ilmenite titanates are much lower than for the materials discussed above. (For ceramic $MgTiO_3$, for example, the low-frequency dielectric constant is 13.9.[49]) This is expected on the basis of the observed infrared spectra, where the bands are less intense and less clearly defined than in the perovskite titanates.

CHAPTER V

CONCLUSIONS

The infrared spectrum of thin single-crystal $BaTiO_3$ has absorption bands located at 495 cm^{-1} and about 340 cm^{-1}, due to normal vibrations of the TiO_3 group. On the basis of the number of degrees of freedom of the unit cell, a low-frequency band is expected, arising from a vibration of the Ba ion against the TiO_3 group. The frequency of this vibration has been estimated to be about 225 cm^{-1} by comparing the specific heat contributions of the observed vibrations with the measured low-temperature specific heat.

The slight frequency difference observed between the tetragonal and the cubic spectra and the frequency difference for vibrations along and at right angles to the polar axis in the tetragonal phase are due to the slight shift of the Ti ion from a central position in the unit cell when the material becomes ferroelectric. Band splitting in the orthorhombic and rhombohedral phases is in agreement with that expected from the lowered symmetry of these phases. No abnormal intensity differences have been observed between the spectra of the various phases. The observed spectra can thus be explained on the basis of known atomic positions and reasonable interatomic forces, with no anomalous effects due to ferroelectricity per se.

The observed similarity of the spectrum of $BaTiO_3$ to that of the other perovskite titanates and niobates investigated is expected, since the observed bands are due to a motion primarily of oxygen ions. The force constants obtained by the approximate treatment used lead to

reasonable agreement with measured elastic constants.

Further experimental work on the absorption spectrum of $BaTiO_3$ will depend on the development of far infrared spectrophotometers of much higher sensitivity. Detailed measurements on single crystals for the band centered at about 340 cm^{-1} would be of interest. The high reflectivity of $BaTiO_3$ in this region will make such measurements difficult to carry out.

Measurements on the spectrum to frequencies of about 200 cm^{-1} would permit an accurate determination of the frequencies of the three bands, and justify the extension of the two force constant treatment employed in this investigation to a three force constant treatment. More exact normal co-ordinate motions could then be determined, and the vector sum of the dipole moment change with interatomic distance separated into individual bond contributions. Accurate information thus obtained would be of great value in the development of a quantitative theory of the nature of the ferroelectric state in $BaTiO_3$.

Further investigations of the observed frequency shift between single-crystal spectra and the spectra of powdered samples dispersed in pressed disks would be of interest for the general problem of the effect of the local field on the oscillator frequency and transition probability.

APPENDIX A

Determination of the True Transmission Minimum in Thin Single Crystal Absorption Spectra from the Observed Transmission and the Single Surface Reflectivity

Let

s = the fractional amplitude transmitted through the surface

r = the fractional amplitude reflected at the surface

t = the fractional amplitude transmitted through the body of the material.

The amplitudes of the transmitted and reflected waves are shown in Fig. 29.

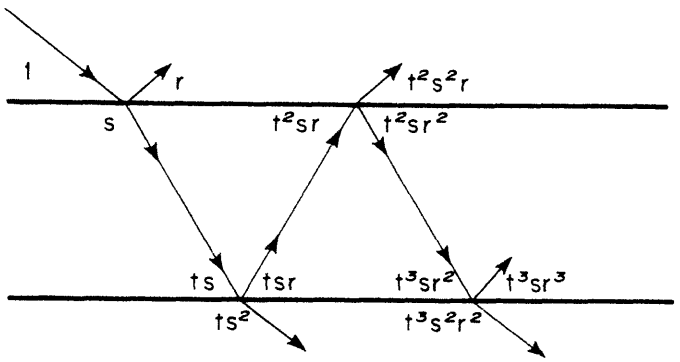

Fig. 29. Thin crystal transmission and reflection.

The amplitude of the transmitted wave d:is:

$$Q = ts^2 \left[1 \pm t^2r^2 + t^4r^4 + t^6r^6 + \ldots \right]$$

$$= \frac{ts^2}{1 \pm t^2r^2} = \frac{t(1 - r^2)}{1 \pm t^2r^2} \quad .$$

(The minus sign is used for the limiting case of constructive interference; the plus sign for destructive interference.)

Change from wave amplitudes to wave intensities, the quantity actually measured.

$$D = (d)^2 = \frac{T(1 - R)^2}{1 \pm TR^2} \qquad \begin{matrix} T = (t)^2 \\ R = (r)^2 \end{matrix}$$

Solve for the transmission T.

$$T = \frac{\xi \mp 2R - \sqrt{(\xi \mp 2R)^2 - 4R^2}}{2R^2} ,$$

where $\xi = \frac{(1 - R)^2}{D}$.

For frequencies near the transmission minimum, where the absorption is large, the following approximation may be made.

$$D \sim \frac{T(1 - R)^2}{1 \pm 2TR}$$

$$T \sim \frac{D}{(1 - R)^2 \mp 2DR}$$

Bibliography

1. A. von Hippel, Revs. Mod. Phys. 22, 221 (1950).
2. A. von Hippel, W. B. Westphal, and P.A. Miles, "Dielectric Spectroscopy of Ferromagnetic Semiconductors," Tech. Rep. 97, July 1955, Laboratory for Insulation Research, Mass. Inst. Tech.
3. R. P. Waldron, Phys. Rev. 99, 1727 (1955).
4. T. Liebisch and H. Rubens, Sitzber. preuss. Akad. Wiss., 1951,p.211.
5. A. von Hippel, R.G. Breckenridge, F. G. Chesley, and L. Tisza, Ind. Eng. Chem. 38, 1097 (1946).
6. R. T. Mara, G.B.B.M. Sutherland, and H. V. Tyrell, Phys. Rev. 96, 801 (1954).
7. C. Hilsum, J. Opt. Soc. Amer. 45, 771 (1955).
8. S.B. Levin, N.J. Field, F.M. Plock, and L. Merker, J. Opt. Soc. Amer. 45, 737 (1955).
9. W. J. Merz, Phys. Rev. 91, 513 (1953).
10. W. J. Merz, Phys. Rev. 76, 1221 (1949).
11. H. D. Megaw, Proc. Roy. Soc. (London) A189, 261 (1947).
12. P. Vousden, Acta Cryst. 4, 373 (1951).
13. R. G. Rhodes, Acta Cryst. 2, 417 (1949).
14. W. Känzig, Helv. Phys. Acta 24, 175 (1951).
15. H. T. Evans, Jr., Tech. Rep. 58, Lab. Ins. Res., Mass. Inst. Tech., January, 1953.
16. B.C. Frazer, H. R. Danner, and R. Pepinsky, Phys. Rev. 100, 745 (1955).
17. G. Shirane and R. Pepinsky, Phys. Rev. 97, 1179 (1955).
18. Downie, Magoon, Purcell, and Crawford, J. Opt. Soc. Amer. 43, 941 (1953).

19. E. L. Wagner and D. F. Hornig, J. Chem. Phys. 18, 296 (1950).

20. M.M. Stimson and M.J. O'Donnel, J. Am. Chem. Soc. 74, 1805 (1952).

21. U. Schiedt and H. Reinwein, Z. Naturforsch. 76, 270 (1952); Appl. Spect. 7, 75 (1953).

22. R. D. Burbank and H. T. Evans, Jr., Acta Cryst. 1, 330 (1948).

23. E. A. Wood, Acta Cryst. 4, 353 (1951).

24. G. Shirane, H. Danner, A. Pavlovik, and R. Pepinsky, Phys. Rev. 93, 672 (1954).

25. G. Shirane, R. Newnham, and R. Pepinsky, Phys. Rev. 96, 581 (1954).

26. J. P. Remeika, J. Am. Chem. Soc. 76, 940 (1954).

27. J. G. Kirkwood, quoted by W. West and R. T. Edwards, J. Chem. Phys. 5, 14 (1937).

28. N.S. Bayliss, J. Chem. Phys. 18, 292 (1950).

29. L. H. Jones and R. M. Badger, J. Am. Chem. Soc. 73, 3132 (1951).

30. N. Q. Chako, J. Chem. Phys. 2, 644 (1934).

31. S. R. Polo and M. K. Wilson, J. Chem. Phys. 23, 2376 (1955).

32. L. E. Jacobs and J.R. Platt, J. Chem. Phys. 16, 1137 (1948).

33. W. Känzig, Phys. Rev. 98, 549 (1955).

34. M. Born and Th. von Karman, Physik. Z. 13, 297 (1912); 14, 15 (1913).

35. G. Herzberg, "Infrared and Raman Spectra," Van Nostrand, 1945, pp. 121 ff.

36. J. Fock, Z. Physik 90, 44 (1934).

37. R. B. Barnes, Z. Physik 75, 723 (1932).

38. C. Kittel, "Introduction to Solid-State Physics," Wiley and Sons, New York, 1953, pp. 65 ff.

39. S.S. Todd and R. E. Lorenson, J. Am. Chem. Soc. 74, 2043 (1952).

40. R. G. Rhodes, Acta Cryst. 4, 105 (1951).

41. W. L. Bond, W. P. Mason, and H. J. McSkimin, Phys. Rev. 82, 442 (1951).

42. F. M. Seitz, "Modern Theory of Solids," McGraw-Hill, 1940, pp. 94 ff.

43. R. S. Mulliken, J. Chem. Phys. 7, 14 (1939).

44. S. Naray-Szabo, Naturwiss. 31, 202 (1943).

45. H. C. Schweinler, Phys. Rev. 87, 5 (1952).

46. B. Szigeti, Trans. Faraday Soc. 45, 155 (1949).

47. M. E. Drougard and D. R. Young, Phys. Rev. 94, 1561 (1954).

48. P. W. Forsbergh, Jr., Phys. Rev. 76, 1187 (1949).

49. "Tables of Dielectric Materials, Vol. IV," Tech. Rep. 57, Laboratory for Insulation Research, Mass. Inst. Tech. January, 1953.

50. W. B. Westphal, private communication.

51. G. Shirane and S. Hoshino, J. Phys. Soc. Japan 6, 265 (1951).

Biographical Note

Born:

Butler, Pennsylvania, on October 18, 1929

Institutions attended:

Butler, Penna., High School	1943-47
University of Rochester	1947-1951 B.S. in Optics
Massachusetts Institute of Technology	1951-56

Scholarships and Fellowships:

Rochester Prize Scholarship	1947-1951
M.I.T. Summer Overseas Fellowship	Summer 1954
I.B.M. Fellowship	1954-56

Professional Experience:

Preston Laboratories, Butler, Penna.	Summers 1947-49
Eastman-Kodak Company, Rochester, New York	Summer 1950
Research Assistant, Laboratory for Insulation Research, Mass. Inst. Technology	1951-1954
Metallografiska Institut, Stockholm, Sweden	Summer 1954

Professional Sociaty Memberships:

American Physical Society	Member
American Optical Society	Member
Sigma Xi	Member